Available online at www.sciencedirect.com
SciVerse ScienceDirect
Geochimica et Cosmochimica Acta 96 (2012) 174–192
Geochimica et Cosmochimica Acta
www.elsevier.com/locate/gca

Diatom silicon isotopes as a proxy for silicic acid utilisation: A Southern Ocean core top calibration

Katherine E. Egan [a,*], Rosalind E.M. Rickaby [a], Melanie J. Leng [b,c], Katharine R. Hendry [d,e], Michaël Hermoso [a], Hilary J. Sloane [b,c], Helen Bostock [f], Alex N. Halliday [a]

[a] Department of Earth Sciences, University of Oxford, Parks Road, Oxford OX1 3PR, UK
[b] Department of Geology, University of Leicester, Leicester LE1 7RH, UK
[c] NERC Isotope Geosciences Laboratory, British Geological Survey, Keyworth, Nottingham NG12 5GG, UK
[d] Department of Marine Chemistry and Geochemistry, Woods Hole Oceanographic Institution, Woods Hole, MA 02543, USA
[e] School of Earth and Ocean Sciences, Cardiff University, Main Building, Park Place, Cardiff CF10 3AT, UK
[f] National Institute of Water and Atmospheric Research, Private Bag 14-901, Wellington 6241, New Zealand

Received 29 September 2011; accepted in revised form 1 August 2012; available online 11 August 2012

Abstract

Despite a growing body of work that uses diatom δ^{30}Si to reconstruct past changes in silicic acid utilisation, few studies have focused on calibrating core top data with modern oceanographic conditions. In this study, a microfiltration technique is used to divide Southern Ocean core top silica into narrow size ranges, separating components such as radiolaria, sponge spicules and clay minerals from diatoms. Silicon isotope analysis of these components demonstrates that inclusion of small amounts of non-diatom material can significantly offset the measured from the true diatom δ^{30}Si. Once the correct size fraction is selected (generally 2–20 μm), diatom δ^{30}Si shows a strong negative correlation with surface water silicic acid concentration ($R^2 = 0.92$), highly supportive of the qualitative use of diatom δ^{30}Si as a proxy for silicic acid utilisation. The core top diatom δ^{30}Si matches well with mixed layer filtered diatom δ^{30}Si from published *in situ* studies, suggesting little to no effect of either dissolution on export through the water column, or early diagenesis, on diatom δ^{30}Si in sediments from the Southern Ocean. However, the core top diatom δ^{30}Si shows a poor fit to simple Rayleigh or steady state models of the Southern Ocean when a single source term is used. The data can instead be described by these models only when variations in the initial conditions of upwelled silicic acid concentration and δ^{30}Si are taken into account, a caveat which may introduce some error into quantitative reconstructions of past silicic acid utilisation from diatom δ^{30}Si.

1. INTRODUCTION

Reliable palaeoproductivity and nutrient utilisation proxies are essential to our knowledge of the role played by the marine biosphere in climatic change. Such records are of particular importance in regions such as the Southern Ocean, the Equatorial and Sub-Arctic Pacific, and areas of coastal upwelling which have a direct influence on atmospheric CO_2 concentration and are sensitive to changes in biological carbon pumping (Sarmiento and Toggweiler, 1984; Elderfield and Rickaby, 2000; Sigman and Boyle, 2000; Takahashi et al., 2002; Kohfeld et al., 2005; De La Rocha, 2006). In these areas, a lack of carbonate preservation limits the use of traditional nutrient utilisation or productivity proxies based on foraminifera (e.g. Benthic Foraminiferan Accumulation Rates, δ^{13}C) (Swann and

* Corresponding author. Address: National Oceanography Centre, Southampton, University of Southampton Waterfront Campus, European Way, Southampton, SO14 3ZH, UK. Tel.: +44 238059 6573; fax: +44 1865 272072.
E-mail address: K.E.Egan@soton.ac.uk (K.E. Egan).

0016-7037
http://dx.doi.org/10.1016/j.gca.2012.08.002

Leng, 2009). As a result we must turn to less conventional media, such as biogenic silica, to gain insight into past variation in nutrient utilisation.

Diatoms, siliceous walled phytoplankton, are the dominant contributor to modern biogenic silica deposition (Tréguer et al., 1995). Diatoms play an important role in carbon export; in nutrient rich and coastal environments they may account for up to 75% of primary production (Nelson et al., 1995; De La Rocha et al., 1998). Their silica frustules also provide an effective ballast material for sinking organic matter (Buesseler, 1998; Baines et al., 2010). As primary producers making a significant contribution to the biological carbon pump, and which have an absolute requirement for silicon, diatoms represent an important link between the silicon and carbon cycles.

The silicon isotope signature preserved in diatom opal may be used as a proxy for their silicic acid utilisation (De La Rocha et al., 1997, 1998, 2006). During silicification diatoms biologically discriminate against the heavier Si isotopes (^{30}Si and ^{29}Si) with a fractionation factor ($^{30}\varepsilon$) of $-1.1 \pm 0.4‰$ (De La Rocha et al., 1997; Milligan et al., 2004). This imparts a high δ^{30}Si ($\delta^{30}\text{Si} = ([(^{30}\text{Si}/^{28}\text{Si})_{\text{sample}}/(^{30}\text{Si}/^{28}\text{Si})_{\text{std}}] - 1) \times 1000$]) signature on surface water silicic acid, and hence on subsequent diatom silica which forms from it. At depth, remineralisation of diatom silica releases silicic acid with a lower δ^{30}Si than the surface silicic acid, and creates a gradient between high δ^{30}Si, low silicic acid surface water and high silicic acid, low δ^{30}Si deep water. Upwelling re-supplies the high silicic acid, low δ^{30}Si water to the surface ocean. Diatom δ^{30}Si is therefore a measure of diatom silicic acid utilisation, which is itself a balance between the amount of diatom silicification and the rates/composition of upwelled water. This is the basis of the diatom δ^{30}Si proxy, where high δ^{30}Si represents high utilisation. However, diatom δ^{30}Si is still a developing proxy, with areas of both methodology and calibration that require some refinement.

One important caveat is that the impact of non-diatom components on diatom δ^{30}Si measurements is under-constrained. Due to their small size, it is generally considered impractical to hand-pick diatom frustules (Swann et al., 2008) and a sequence of chemical and physical separation techniques are instead employed to purify diatom material (e.g. Morley et al., 2004). However, samples will almost always contain some level of non-diatom material (Morley et al., 2004; De La Rocha, 2006; Leng and Barker, 2006; Swann and Leng, 2009). Non-diatom components may contribute silica with significantly different δ^{30}Si to diatom opal, for example sponges are known to fractionate silicon with $^{30}\varepsilon$ up to approximately $-4‰$, much greater than that of the diatoms (De la Rocha, 2003; Hendry et al., 2010). Assessment of the effect of non-diatom sedimentary components on measured δ^{30}Si is therefore required to ensure the reliability of silicic acid utilisation records based on diatom δ^{30}Si.

Additionally, little work has been undertaken to establish how well modern sedimentary diatom δ^{30}Si reflects silicic acid utilisation in the surface ocean or the associated uncertainties involved in reconstructing utilisation from downcore records (De La Rocha et al., 2011; Fripiat et al., 2011b). The δ^{30}Si of both silicic acid and diatom opal may be described using either a Rayleigh or steady state fractionation model (e.g. De La Rocha et al., 1998). Rayleigh fractionation considers the surface ocean to have a finite pool of silicic acid that is progressively depleted by diatoms and exported to the deep ocean. With increasing export both silicic acid and diatom δ^{30}Si become progressively higher. In the steady state model, a continuous supply of silicic acid from the deep ocean to the surface is matched by diatom uptake and export. These models may allow the reconstruction of past changes in surface water silicic acid utilisation by diatoms, but require knowledge of the initial conditions from which fractionation occurs i.e. the starting silicic acid concentration and its δ^{30}Si value. It is currently not clear whether such models, with one fixed set of initial conditions, are applicable over large areas of the modern ocean, and if so, which are the most appropriate starting conditions to use in reconstructions. To this end, a body of work has been published on the δ^{30}Si of both silicic acid and filtered biogenic opal (De La Rocha et al., 2000; Varela et al., 2004; Cardinal et al., 2005, 2007; Beucher et al., 2008, 2011; Reynolds et al., 2008; Fripiat et al., 2011a,b,c), but despite this, opinion is divided over whether the Southern Ocean may be modelled as a single system. Given the growing number of oceanic studies available for comparison, the step of core top calibration is overdue.

Here, we aim to develop the diatom δ^{30}Si proxy both in terms of methodology and calibration, which, especially if used in combination with other proxies such as the δ^{30}Si of sponge spicules (deep water silicic acid concentration (De La Rocha et al., 1997, 2003; Hendry et al., 2010)), and diatom δ^{15}N (nitrate utilisation (Sigman et al., 1999; Brzezinski et al., 2002; De La Rocha, 2006)), has great potential for the reconstruction of past productivity and nutrient dynamics. Core top calibration of the Southern Ocean, representing a first assessment of the contribution made by different components to measured δ^{30}Si, is presented. Through comparison of this latitudinal transect of core top diatom δ^{30}Si with modern surface water silicic acid concentrations, the extent to which simple models may allow quantitative reconstruction of past silicic acid utilisation is assessed.

2. MATERIALS AND METHODS

2.1. Materials

We have analysed sediments from both the Atlantic and Pacific sectors of the Southern Ocean covering a range of silicic acid concentrations from annual averages of ~80 μM in the Firth of Tay (NBP07-03-KCO8A) to ~10 μM just north of the Polar Front (TAN0803-127) (Fig. 1, Table 1). The Western Antarctic Peninsula cores, JCR112-BC383 (383), JCR112-BC385 (385) and JCR112-BC391 (391) were collected as part of an Antarctic Funding Initiative Project (AFI4-02) in collaboration with the Rothera Biogeochemical Time Series (Hendry and Rickaby, 2008). They represent approximately 10 years of modern sediment accumulation, as evidenced by: (i) the

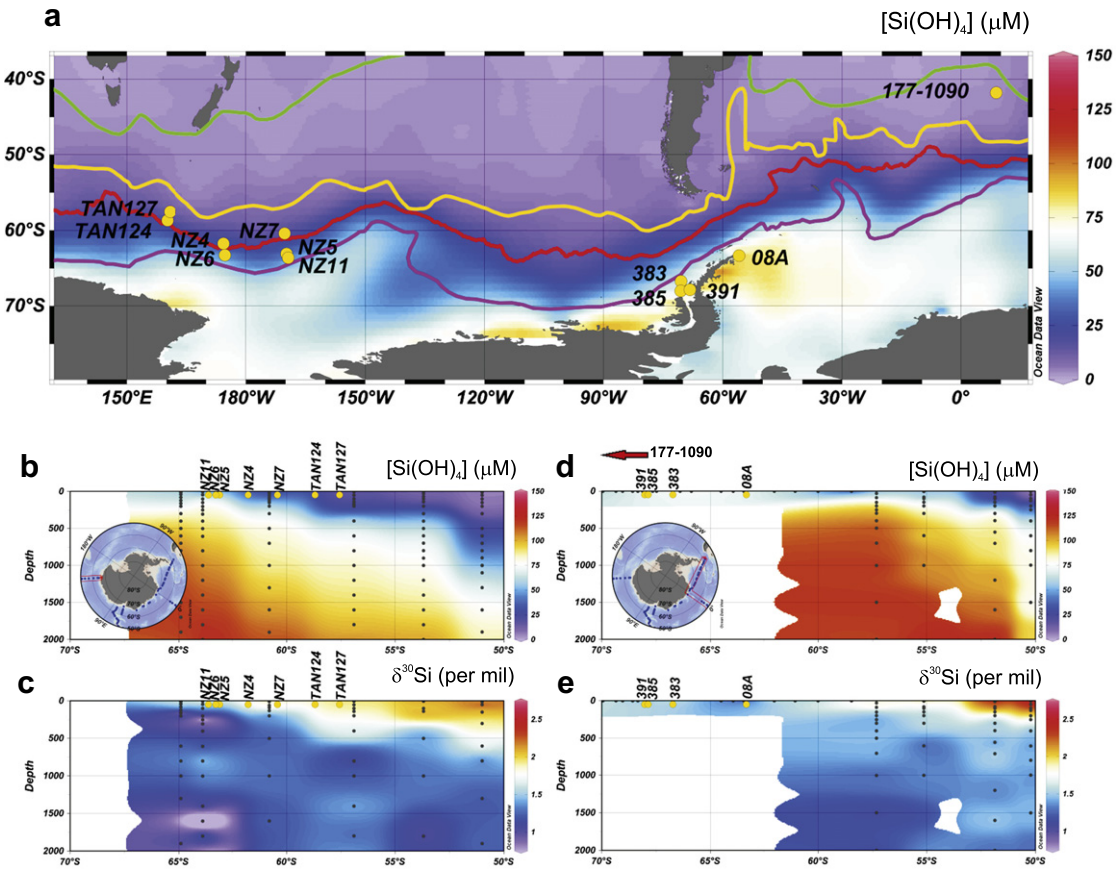

Fig. 1. (a) Core top locations with annual surface water silicic acid concentration (World Ocean Atlas, 2009, http://www.nodc.noaa.gov/OC5/WOA05pr_woa05.html) and Southern Ocean Antarctic Circumpolar Current (ACC) Fronts (Orsi, 1995). Purple = ACC Southern Boundary (SB), Red = Polar Front (PF), Yellow = Sub-Antarctic Front (SAF), Green = Sub-Tropical Front (STF); (b and c) Pacific Sector Silicic acid concentration and δ^{30}Si, respectively, above 2000 m (Cardinal et al., 2005) with core top locations plotted at respective latitude; (d and e) Atlantic Sector Silicic acid concentration and δ^{30}Si, respectively, above 2000 m (De La Rocha et al., 2011; Fripiat et al., 2011b) with core top locations plotted at respective latitude. Note Core tops are compared to the nearest transect available and that as such longitudes are not exactly the same. (For interpretation of the references to colour in this figure legend, the reader is referred to the web version of this article.)

presence of photo-detrital fluff near site 383, and (ii) sedimentation rates of 0.14 cm/yr and 0.13 cm/yr at two proximal sites (^{210}Pb dating, 391 and JCR112-BC388 (388) respectively in Hendry and Rickaby (2008)). NBP07-03-KCO8A (08A) was collected as part of the 2006 SHADRILL II cruise to the north-western Weddell Sea; its top has been ^{14}C dated to 1706AD. Samples from the Pacific sector of the Southern Ocean were supplied by the New Zealand National Institute of Water and Atmospheric Research (TAN0803-127 (TAN127) and TAN0803-124 (TAN124)) and Oregon State University (in subsequent text 'NZ samples': KN7812-04BC (NZ4), NBP9802-05MC1 (NZ5), KN7812-06BC (NZ6), NBP9802-07MC1 (NZ7), KN7812-11BC (NZ11)) and have been ^{14}C dated to <10 k years.

To test the relationship between geological samples and core top size fractions, we have analysed four downcore samples from the Eocene and Oligocene of Ocean Drilling Program Site 177-1090 in the Atlantic Sector of the Southern Ocean (Table 1). The site has a palaeodepth of 3700 m and is currently situated just south of the Subtropical Front. The age model is from Channell et al. (2003) on the timescale of Cande and Kent (1995).

2.2. Methods

2.2.1. Biogenic silica extraction and size separation

Biogenic opal was separated from sediments using both chemical and physical techniques following the protocol of Hendry and Rickaby (2008), adapted from the methods of Shemesh et al. (1995 onwards), Ellwood and Hunter (1999), and Morley et al. (2004), with the addition of the novel microseparation technique of Minoletti et al. (2009). The eight stage methodology is outlined in Fig. 2 and described below.

2.2.1.1. Chemical cleaning stage 1 and heavy liquid separation. Initial chemical cleaning steps used H_2O_2 and HCl to remove organic matter and carbonate respectively. This was followed by several heavy liquid separations using sodium

Table 1
Core site summary.

Site (text reference)	Latitude	Longitude	Depth (m)	Age	Modern annual silicic acid range and (annual average) (μM)	Core type	Source
JCR112–BC383 (383)	−66.72	−70.44	578	Modern accumulation (photodetrital fluff)	34–74 (57)	Box	AFI 4/02
JCR112–BC385 (385)	−68.02	−70.52	845	<10 years (^{210}Pb)	43–92 (72)	Box	AFI 4/02
JCR112-BC391 (391)	−67.86	−68.23	814	<10 years (^{210}Pb)	55–65 (60)	Box	AFI 4/02
NBP07-03–KC08A (08A)	−63.34	−55.87	629	1706AD (^{14}C)	76–101 (88)	Kaston	Shadrill
TAN0803-124 (TAN124)	−58.69	160.23	4358	47600 ± 1800 radiocarbon years at 11 cm	7–26 (17)	Gravity	NIWA
TAN0803-127 (TAN127)	−57.56	160.87	3830	7567 ± 100 radiocarbon years at 1 cm	4–20 (12)	Gravity	NIWA
KN7812-04BC (NZ4)	−61.77	174.42	4240	<10 Ka (^{14}C)	3–39 (24)	Box	OSU
NBP9802-05MC1 (NZ5)	−63.11	−169.74	2927	<10 Ka (^{14}C)	19–53 (39)	Multi	OSU
KN7812-06BC (NZ6)	−63.29	174.78	2429	<10 Ka (^{14}C)	22–58 (40)	Box	OSU
NBP9802-07MC1 (NZ7)	−60.42	−170.19	3860	<10 Ka (^{14}C)	6–31 (18)	Multi	OSU
KN7812-11BC NZ11)	−63.63	−169.32	2738	<10 Ka (^{14}C)	19–53 (39)	Box	OSU
ODP177-1090B	−41.81	8.9	3700 m (palaeodepth)	25.5 Ma, 27.1 Ma, 33.8 Ma, 35.9 Ma	N/A	Hydraulic piston core/ extended core barrel	Ocean drilling program

polytungstate (SPT, $8Na_2WO_4WO_3{\cdot}H_2O$) to remove clastic grains and clay minerals. After each stage opal was thoroughly rinsed with deionised water to remove any traces of reagents or heavy liquid.

2.2.1.2. Microseparation. In traditional methods, sieving is employed either before or after initial chemical cleaning with the aim of removing clay minerals and the siliceous components of other organisms such as radiolaria and sponges (e.g. Shemesh et al., 1988; Morley et al., 2004). Here, rather than sieving, which is difficult below 63 μm, we have employed a microfiltration technique (described in Minoletti et al., 2009), which allowed us to separate the samples into a range of size fractions between 2 and 100 μm. The technique involves filtering sediment suspensions through a series of nylon meshes or Millipore® polycarbonate membranes with the aid of an ultrasonic bath (Fig. 3). The gentle ultrasonication continuously re-suspends the sediment and prevents clogging of the membrane/mesh, ensuring effective separation. Separations were made at 50 or 41, 20, 12, 8, 5 and 2 μm, and a sample of the bulk silica (purified silica prior to size fraction separation) was removed for analysis. As only the <63 μm fraction was available from the NZ samples (Table 1), separations for these samples were made at 2 and 20 μm. Size fractions were dried and weighed. Smear slides of each fraction were analysed for relative proportions of diatoms to other siliceous organisms, as well as for diatom specific abundances. If at this stage any clastic grains were observed, a repeat heavy liquid separation was undertaken. For 08A some clastic contamination proved impossible to remove.

For the Antarctic Peninsula sites, a comparison of bulk silica (i.e. no microseparation) with separated diatom size fractions, using a scanning electron microscope, showed that the microseparation removed clay minerals which were adhered to and clogging the pores of frustules in the bulk samples (Fig. 4). At all sites, optical and SEM observations of the <2 μm fraction showed abundant clay.

Fragmentation of siliceous components limits the ability of microseparation to partition them on merit of their size and/or shape. Fragmentation has two sources; initial fragmentation during sinking and early diagenesis, and fragmentation occurring during ultrasonication as part of the microseparation technique. Initial fragmentation is particularly high in coastal Antarctic Peninsula samples, while the Pacific sector samples tend to have relatively low numbers of fragments. To determine optimal sonication settings and potential fragmentation, an experiment subjecting whole diatom valves to different levels of sonication, over various lengths of time, was undertaken (Electronic Annex 1). This shows that fragmentation is directly related to both time and power setting, but that use of the lowest power setting on the ultrasonic bath minimises fragmentation during microseparation.

2.2.1.3. Chemical cleaning stage 2 (Oxford only). Silicon isotope analyses were conducted at both Oxford University and at the NERC Isotope Geochemistry Laboratory, Nottingham (NIGL). The latter facility was used for some samples as they were able also to analyse oxygen isotope ratios from the same samples (data not shown here). Si isotope data from the two laboratories have been shown to be comparable (Hendry et al., 2010). The samples analysed in Ox-

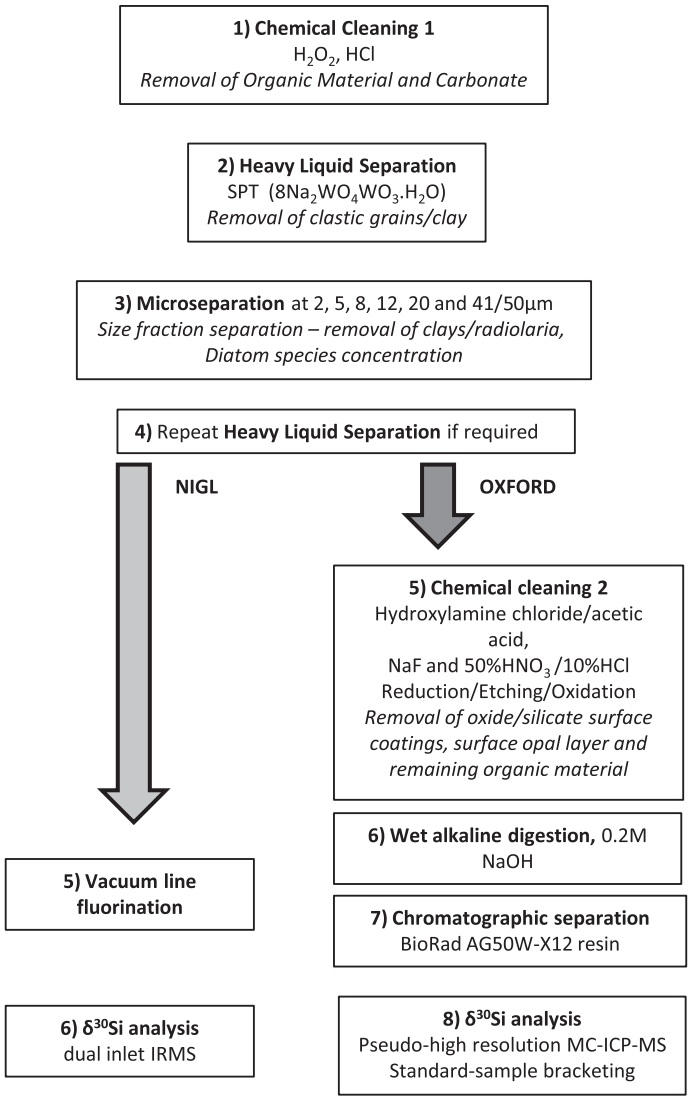

Fig. 2. Summary of methods. Steps 1 to 4 are biogenic silica purification techniques common to analyses performed both in Oxford and at NIGL. Steps 5 and 6 (left hand side) are NIGL analysis steps and 5 to 8 (right hand side) are clean up steps and analysis techniques used in Oxford. SPT = Sodium Polytungstate. MC-ICP-MS = Multi-collector inductively coupled plasma mass spectrometer.

ford underwent an additional chemical cleaning stage, following the protocol of Ellwood and Hunter (1999) (Fig. 2). This involves reductive cleaning (hydroxylamine hydrochloride/acetic acid solution), etching (NaF) and oxidative cleaning (strong acid solution of 50% HNO_3/10% HCl), to remove any remaining organic matter and surface contaminants respectively. This was not required for NIGL due to the different isotope extraction methods (see Section 2.2.1.5 below).

2.2.1.4. Digestion and chromatographic separation (Oxford only). The purified opal was dissolved via wet alkaline digestion (Ragueneau et al., 2005; Cardinal et al., 2007) in 0.2 M NaOH at 100 °C for 40 min. The samples were then acidified to pH ~2 with 0.2 M thermally distilled HCl and separated from major ions using cation exchange resin (BioRad AG50W-X12) (Georg et al., 2006).

2.2.1.5. Vacuum line fluorination (NIGL only). At NIGL a fluorination method was employed to convert the silica into SiF_4 (and O_2) using a fluorine based reagent. The diatom silica was reacted in three steps, and subsequently the Si was extracted. Stage one involved 'outgassing' (dehydration) to remove surficial and loosely bound water in the reaction tubes at room temperature. Stage two involved a prefluorination step with a stoichiometric deficiency of the reagent (BrF_5) at low temperature which removes the hydroxyl and loosely bound water. The third stage was a total reaction at 450 °C for 12 h with an excess of reagent to dissociate the silica into O_2 and Si (as SiF_4) (Leng and Sloane, 2008).

2.2.1.6. Mass spectrometry and δ^{30}Si analysis. At Oxford, δ^{30}Si analysis was carried out using a Nu Instruments Nu-Plasma HR multi-collector inductively coupled plasma mass

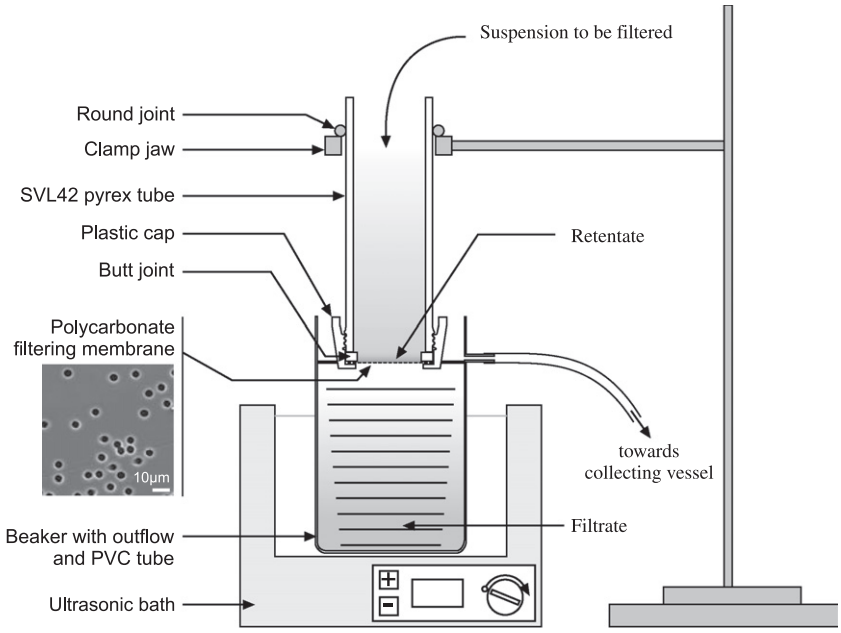

Fig. 3. Ultrasonic filtration setup, Figure from Minoletti et al. (2009). The opal suspension is poured into the Pyrex tube. Larger particles are retained on either a polycarbonate membrane (<20 μm) or nylon mesh (20–100 μm). The filtrate is collected and can then be re-filtered at a smaller size if required. A variable power ultrasonic bath is used to minimize valve fragmentation (see Electronic Annex 1 for more information on fragmentation during ultrasonication).

spectrometer (HR-MC-ICP-MS). Samples were introduced via a self-aspirating PFA microconcentric nebuliser (ESI) in a Cetac Aridus II desolvating unit. The HR-MC-ICP-MS was run in medium resolution mode ($m/\Delta m$ ~3500) in order to resolve interferences on ^{29}Si and ^{30}Si. Standard-sample bracketing was used to account for mass bias, and eight repeats of 20 × 8 s integrations were made. Samples were measured relative to the NIST RM 8546 standard. The Diatomite standard (1.26‰ ± 0.2‰ (2σSD), Reynolds et al., 2007) was analysed with each batch of samples. From this, our long term reproducibility is 0.24‰ (2σSD, $n = 52$), with a mean of +1.26‰ an average internal error of 0.18‰ (2σSD of the eight repeat standard sample measurements).

At NIGL $\delta^{30}Si$ measurement was carried out using a Thermo-Finnigan MAT253 gas source mass spectrometer. The gaseous silicon tetrafluoride (SiF_4) was produced off line and introduced via a manifold. Samples were again measured relative to NIST RM 8546. The diatomite standard BFC (Chapligin et al., 2011) was run with each batch of samples to calibrate the sample data. From this, our long term reproducibility is 0.2‰ (2σSD). Duplicate samples had a mean reproducibility of 0.06‰ (2σSD). All measurement values quoted in the text and figures have error values equal to the 2σSD external reproducibility, except where the internal reproducibility was greater, in which case this is quoted instead.

2.2.1.7. Size fraction composition analysis. Area analysis of smear slides images (taken with a high-resolution Zeiss™ Scope A1 optical microscope and Zeiss AxioCam ICc1 camera) for both diatom to non-diatom component ratios and diatom species were carried out using ImageJ software (free to download from http://rsb.info.nih.gov/ij/index.html). It is noted that there are significant errors associated with area analysis, particularly due to differences in biovolume between the various components (especially between diatoms and radiolaria/sponge spicules).

3. RESULTS

In order to determine the size fraction most appropriate to use to represent diatom $\delta^{30}Si$ in future downcore studies, it is necessary to consider the mass, composition and isotope signature of each size fraction.

3.1. Size fraction mass

For sites on the Antarctic Peninsula (383, 385, 391 and 08A), the <2 μm fraction contained the greatest mass of silica, ranging from 40% at 383 to 70% at 08A (Fig. 5a and b). In contrast, sites in the Pacific sector of the Southern Ocean had <2 μm fractions which contained <1% (TAN124) to 15% (NZ4, TAN127) of the total (Fig. 5c and d). SEM observations of the <2 μm fraction showed it to contain significant amounts of clay at all sites.

The Antarctic Peninsula sites display a general decrease in the amount of silica contained in a size fraction with increasing size e.g. from 15% in the 2–5 μm size fraction, to <1% in the >50 μm at site 383 (Fig. 5a and b). However, there is a small relative peak in silica mass in the 8–12 or 12–20 μm size fractions at all four sites (e.g. 25% in the 12–20 μm at site 383). For TAN127 and 124, there is a decrease in the mass of silica from 35% and 70% (respectively) in the 2–5 μm fractions, to 5% in the 12–20 μm fractions

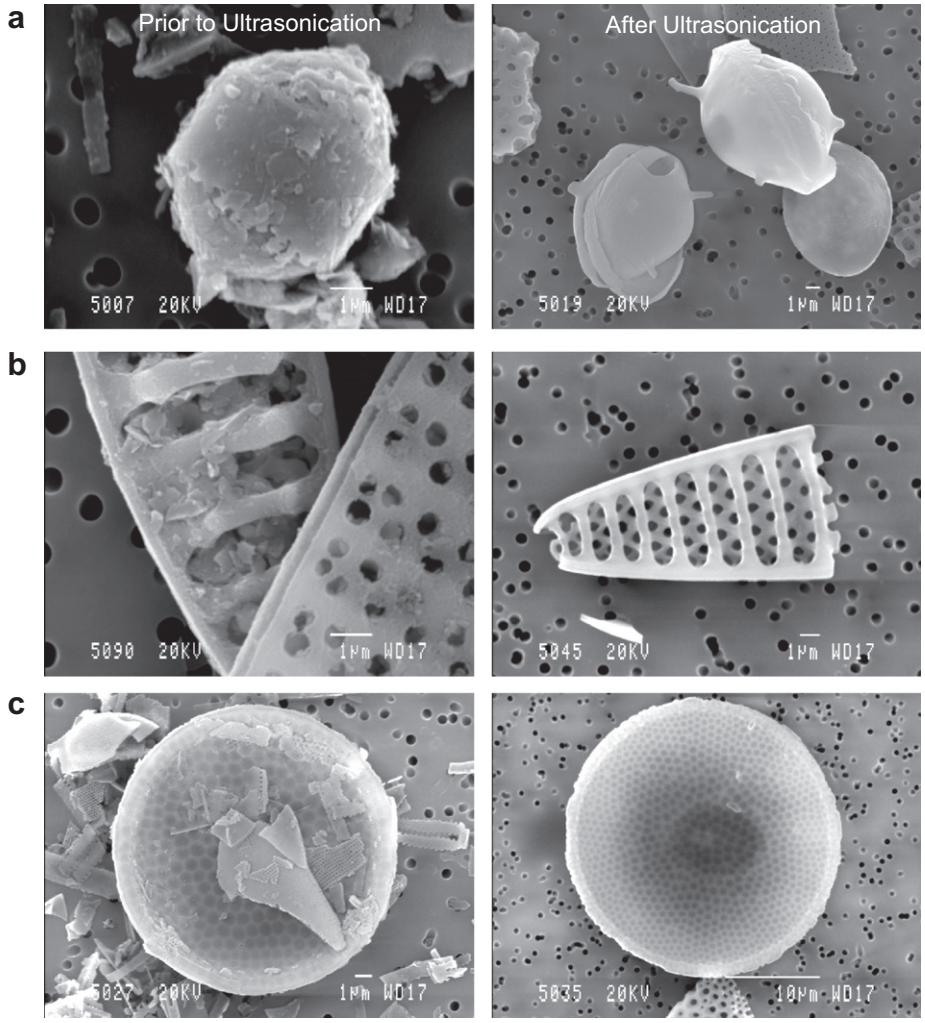

Fig. 4. SEM images of diatoms before (left) and after (right) microseparation (a) *Cheatoceros* resting spores; (b) *Fragilariopsis kerguelensis* and; (c) *Thalassiosira* sp. Images demonstrate the removal of adhered clays and clays lodged in the pores of diatom frustules (particularly b). Images from Antarctic Peninsula sites.

(Fig. 5c). The >50 μm fractions contain 5% of the total at sites TAN127 and TAN124 respectively, in contrast to the <1% found in the >50 μm fraction at any of the Antarctic Peninsula sites. For the NZ sites most silica is contained in the 2–20 μm size fraction which contributes between 75% (NZ7) and 90% (NZ11) to the total mass of silica (Fig. 5d).

In the downcore samples, 1090-18, 26 and 31 have 20% to 25% of material contained in the <2 μm size fraction, compared to 65% in 1090-20. The 2–10 μm size fraction contains between 20% (1090-20) and 55% (1090-26), the 10–20 μm size fraction between 6% (1090-20) and 25% (1090-31) and the 20–41 μm size fraction up to ~10% (1090-26).

3.2. Size fraction composition

At all of the core top sites studied for a full range of size fractions, relative diatom abundance shows the same trend, with diatom percentage lowest in the two largest size fractions (Fig. 6) and closer to 100% in the smaller size fractions (2–20 μm). The small size of material and dominance of clay in the <2 μm fractions meant it was not possible or informative to carry out area analysis, and they are not considered further.

For the Antarctic Peninsula sites (Fig. 6a–c), diatom percentage is highest between 2 and 20 μm, in all cases being between 90% (e.g. site 383, 8–12 μm) and 100% (e.g. site 385, 2–5 μm, 5–8 μm, 12–20 μm). The non-diatom contribution between 2 and 20 μm comprises (in the case of sites 383 and 385) radiolaria, sponge spicules and silicoflagellates. Individually these components never account for more than 5%. In the 2–20 μm range at 08A, the non diatom material is dominantly clastic grains, with a small contribution from sponge spicules. The percentage of diatom material decreases significantly in the larger size fractions, dropping to only 5% in the >50 μm fraction of site 383 and the >41 μm of site 08A (the >50 μm fraction contained almost no material at site 385 and so was not analysed). The diatom percentage contained in the 20–50/20–41 μm fractions falls between that of the 2–20 μm and >50/41 μm fractions, containing 55% to 80% diatom material

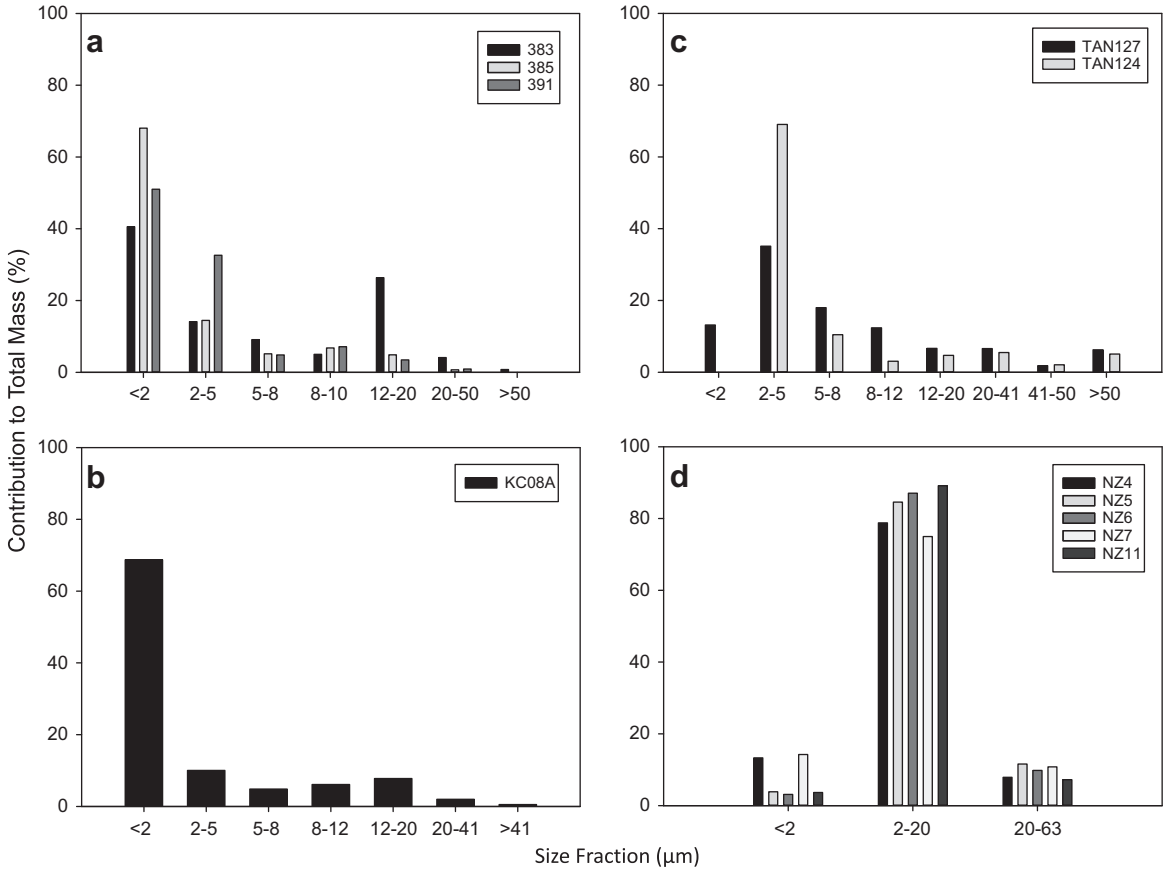

Fig. 5. Size fraction contributions to total silica (% by mass) for; (a) Sites 383, 385 and 391, and; (b) Site 08A on the Antarctic Peninsula; (c) Pacific Sector sites TAN127 and 124, and; (d) Pacific Sector NZ sites. For sites on the Antarctic Peninsula, the <2 μm size fraction contains the most silica, and subsequently silica contribution decreases with increasing size fraction. For Pacific sites TAN127 and 124, the greatest mass is contained in the 2–5 μm fraction, and contribution again decreases with increasing size. NZ sites all have the most opal contained in the 2–20 μm fraction.

at 08A and 383, 385 respectively. At all sites except 08A the largest size fraction is dominated by radiolaria, which contribute up to 95% of silica (e.g. >50 μm fraction at site 383). At 08A, clastic grains account for 65% of the >41 μm fraction.

At TAN127, the pattern is again very similar (Fig. 6d), although diatoms are more abundant in the 20–41 μm fraction, accounting for approximately 90% of the silica. Non-diatom material in all size fractions is almost exclusively radiolarian, and constitutes 94% of the >50 μm size fraction. NZ samples were only analysed in the 20–63 μm range, but are dominantly diatom material (82% at NZ4 to 99% at NZ6). Non-diatom material is generally radiolarian (e.g. 16% at NZ4), with minor contributions from sponge spicules and silicoflagellates.

3.3. Silicon isotope compositions

Size fractions in the range 2–20 μm have a higher average δ^{30}Si of $+0.97 \pm 1.20‰$ with values ranging from $-0.47 \pm 0.24‰$ (08A, 12–20 μm) to $+1.99 \pm 0.26‰$ (TAN124, 8–12 μm), than size fractions >20 μm which average $+0.23‰ \pm 1.97‰$ and range from $-1.84 \pm 0.20‰$ (391, >50 μm) to $+1.4 \pm 0.24‰$ (TAN124, 41–50 μm) (Fig. 7). In general the greatest disparity is between the 2–5 μm fraction and the largest size fraction (>41 or >50 μm) e.g. at site 383 the 2–5 μm fraction has δ^{30}Si of $+1.04 \pm 0.20‰$ and the >50 μm a δ^{30}Si of $-1.21 \pm 0.24‰$. δ^{30}Si of the 2–5 μm, 5–8 μm, 8–12 μm and 12–20 μm fractions is high and stable, with these size fractions being within at least external error at all sites except 08A where the 12–20 μm fraction is significantly lower (Fig. 7). The δ^{30}Si of the <2 μm fractions is lower than that measured in the 2–20 μm (e.g. $-1.14 \pm 0.24‰$ for KC08A) at all sites except TAN127 where it is more positive ($+2.35 \pm 0.31‰$). There was insufficient material in the <2 μm fraction at TAN124 for analysis.

The NZ 2–20 μm δ^{30}Si ranges between $+1.14 \pm 0.24‰$ at NZ6 and $+1.94 \pm 0.24‰$ at NZ4 (Fig. 9, Electronic Annex 2). At NZ4 and NZ5, the 20–63 μm fractions are significantly lower than the 2–20 μm, with offsets of 1.22‰ and 0.63‰ respectively. At sites NZ6 and NZ11 there is no resolvable offset between the two.

All four 1090 downcore samples have 20–41 μm fractions with significantly lower δ^{30}Si values than the 2–10 μm fraction by between 1.79‰ (1090-18) and 1.19‰ (1090-26) (Fig. 8). For two samples, 1090-18 (25.5 Ma) and 1090-20 (27.1 Ma), the 10–20 μm size fraction was also

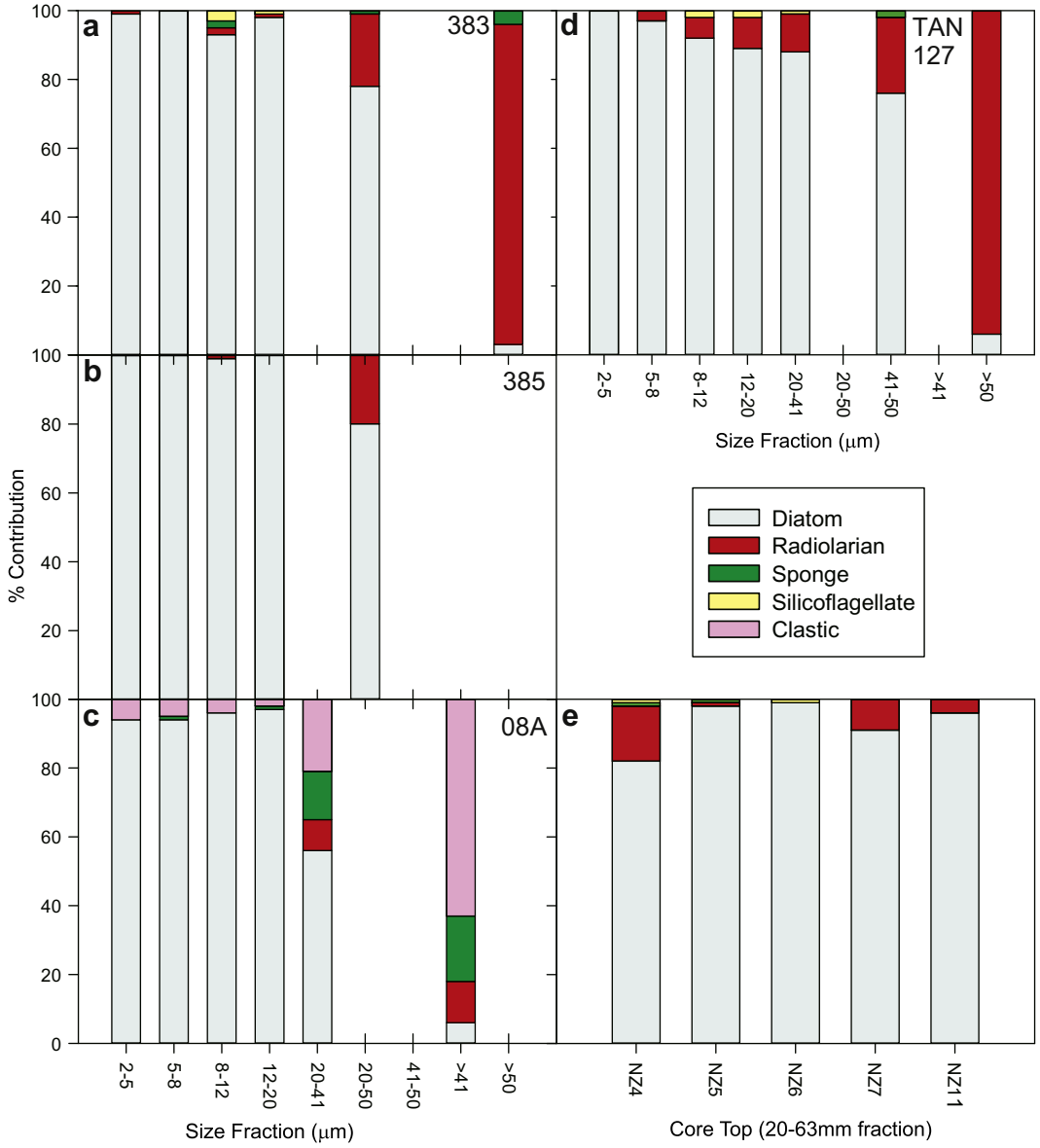

Fig. 6. Size fraction composition by area analysis; (a) Site 383; (b) Site 385; (c) Site 08A; (d) Site TAN127; and (e) 20–63 μm size fractions only for NZ sites; (a–d) Total diatom percentage is lowest in the >50 μm size fraction, which is dominated by radiolaria (or clastic grains at site 08A (c)), and is highest between 2 and 20 μm.

analysed, and is within error of the 2–10 μm fraction, e.g. for 1090-18, 2–10 μm $\delta^{30}Si = +1.87 \pm 0.24‰$, 10–20 μm $\delta^{30}Si = +1.87 \pm 0.24‰$.

4. DISCUSSION

4.1. Size fraction selection for diatom $\delta^{30}Si$ records

It is clear from Figs.7–9 that a consistent relationship exists between the size fraction of silica analysed and $\delta^{30}Si$. The smallest (<2 μm) and largest (>approximately 20 μm) size fractions tend to have lower $\delta^{30}Si$ than those between 2 μm and approximately 20 μm (although the exact size-$\delta^{30}Si$ association differs slightly at TAN127 and 08A). Size fractions with lower $\delta^{30}Si$ contain non-diatom silica which is variably composed of radiolarian tests, sponge spicules, lithogenic components and clay minerals (Figs. 6 and 7), consistent with published $\delta^{30}Si$ ranges of the components present (Fig. 10). Using the size fraction $\delta^{30}Si$ values and area analyses presented in this study, the size range which most robustly represents diatom $\delta^{30}Si$ at each site can be established, and the potential for these non-diatom components to bias diatom $\delta^{30}Si$ assessed.

The $\delta^{30}Si$ of the <2 μm fraction at sites on the Antarctic Peninsula ($-1.14 \pm 0.24‰$ to $+0.7 \pm 0.20‰$, Fig. 7) is consistent with the fraction being composed of a combination of diatom fragments with a higher $\delta^{30}Si$ (e.g. 2–5 μm $\delta^{30}Si$ $+1.04 \pm 0.20‰$ at site 383) and lower $\delta^{30}Si$ clay minerals (Fig. 10). Douthitt (1982) reports a kaolinite clay with $\delta^{30}Si = +1.9‰$, indicating that the high $\delta^{30}Si$ of the

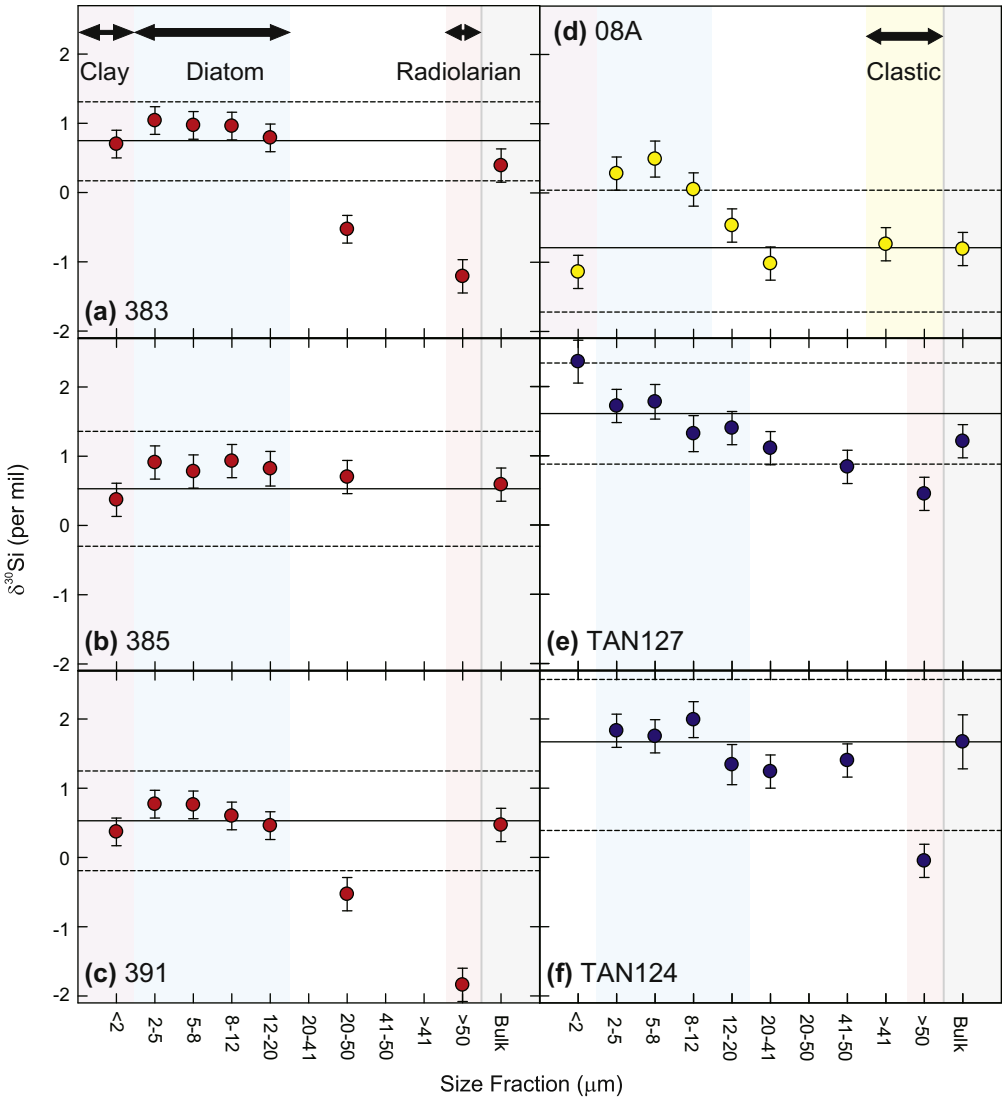

Fig. 7. Core top size fraction δ^{30}Si; (a) Site 383; (b) Site 385; (c) Site 391; (d) Site KC08A; (e) Site TAN127; (f) Site TAN124. Shading denotes areas with δ^{30}Si compositions considered in the text to represent diatoms + clay (pink), predominantly diatom (blue), predominantly radiolaria (orange) and predominantly clastic grains (yellow). Solid lines show estimates of bulk sample δ^{30}Si calculated by mass balance of the individual size fraction δ^{30}Si. Dashed lines show the propagated error on the mass balanced bulk from the 2σSD internal error of the δ^{30}Si of each size fraction, neglecting error on the mass of the size fractions; these bounds therefore represent a minimum estimate of the actual error on this calculation, nevertheless the measured bulk δ^{30}Si is still within error of the calculated bulk δ^{30}Si. (For interpretation of the references to colour in this figure legend, the reader is referred to the web version of this article.)

<2 μm fraction at TAN127 is potentially compatible with Si contribution from clay, but since the <2 μm fraction can contain components other than clay minerals the offset may not be entirely of clay mineral origin. Clay minerals are much more likely to offset diatom δ^{30}Si in sediments such as those from the Antarctic Peninsula, where the <2 μm fraction contributes a large mass of silica to the bulk sample, than the open ocean Pacific sites where it is only a minor component (Fig. 5). Clay minerals adhered to, or lodged in, diatom frustules have been problematic to remove in the past and have required sieving at 10 μm, necessitating the loss of smaller diatom fractions (Morley et al., 2004). This problem can be overcome using the microseparation technique, which effectively dislodges (Fig. 4) and concentrates clays in the <2 μm size fraction.

At 383 and 385 the 2–20 μm size range consists of ⩾90% diatom silica. The size fractions found in this range have the highest δ^{30}Si at their respective site, are all within error of each other, and are considered the most representative of diatom δ^{30}Si. The low δ^{30}Si of the >50 μm fraction at sites 383 and 391 is attributed to the presence of abundant radiolaria (Figs. 6, 7 and 10). On this basis, and considering the low δ^{30}Si of the radiolarian dominated fractions at other our core top sites (Table 2) we suggest that the published range of radiolarian δ^{30}Si extends to lower values than previously documented. The δ^{30}Si of the 20–50 μm size fractions at sites 383 and 391 is intermediate between the 2–20 μm and >50 μm fractions, suggesting that it represents a mixture of diatoms and radiolaria. The area analysis shows this fraction contains around 20% radiolaria at site

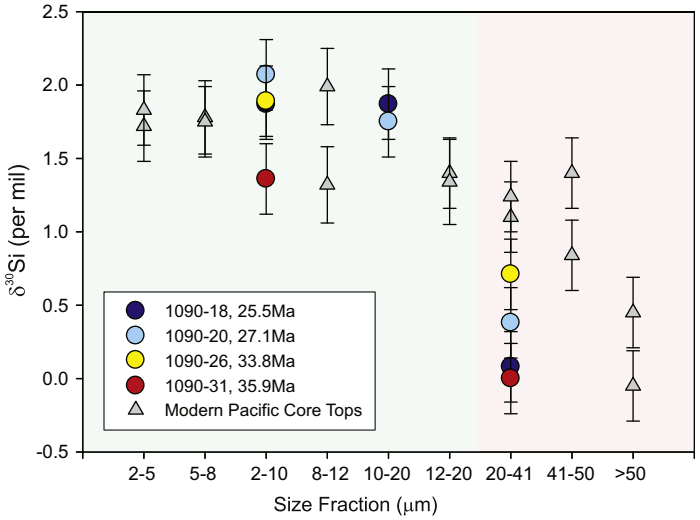

Fig. 8. Size fraction δ^{30}Si from four downcore samples at ODP site 1090 (coloured circles) compared to TAN124 and 127 (grey triangles). Site 1090 and these core tops are located north of the modern Polar Front. The decrease in δ^{30}Si with increasing size fraction observed in modern core tops is also found in downcore samples, despite an age difference of between 26–36 Ma. Additionally, the size-δ^{30}Si relationship is consistent in the downcore samples even across the major climatic shift which occurred at the Eocene–Oligocene Boundary (~34 Ma). Green shading represents the size range considered to represent diatom δ^{30}Si in the downcore samples, and orange shading that considered affected by non-diatom components (dominantly radiolaria). (For interpretation of the references to colour in this figure legend, the reader is referred to the web version of this article.)

383, and from this an expected value for the 20–50 μm fraction can be calculated; a 20% contribution of silica with $\delta^{30}Si = -1.2‰$ (>50 μm δ^{30}Si i.e. radiolaria) to silica with a $\delta^{30}Si = 0.9‰$ (the mass-balanced 2–20 μm δ^{30}Si i.e. diatom) yields a value of +0.5‰, around 1‰ higher than the measured 20–50 μm δ^{30}Si ($-0.53 \pm 0.20‰$). This difference probably occurs for two reasons. Firstly, area analysis is likely to underestimate the contribution of radiolarian silica, since radiolarian tests generally have a larger volume than diatom frustules. Secondly, because of difficulty in the homogenisation of biogenic silica samples, it is possible that heterogeneity in analysed material led to over representation of radiolaria in the measured silicon.

The 2–20 μm range at 08A also contains >90% diatom by area (Fig. 6), in agreement with the highest δ^{30}Si in the 2–5 μm, 5–8 μm and 8–12 μm size fractions. However, the 12–20 μm fraction has significantly lower δ^{30}Si which tends towards the δ^{30}Si of the 20–41 μm and >41 μm fractions (Fig. 7) despite containing significantly more diatom material (Fig. 6). The δ^{30}Si of the 20–41 μm and >41 μm fractions ($-1.02 \pm 0.24‰$ and $-0.74 \pm 0.24‰$) is in keeping with silicon supplied from clastic grains and sponge spicules, although again the 20–41 μm fraction appears to contain significantly more diatom material than the >41 μm fraction. As discussed above, inconsistency between area analysis and measured δ^{30}Si is probably due to inhomogeneous sampling or underestimation of the contribution from non-diatom components by area analysis. In particular, the low δ^{30}Si of the 12–20 μm fraction may be due to sponge spicules, which, because they are generally long and thin could carry a substantial volume of dense silica through a 20 μm mesh. At this site the 2–12 μm fraction is most representative of diatom δ^{30}Si.

At TAN124 and TAN127 a large, radiolarian rich >50 μm size fraction with low δ^{30}Si relative to the smaller, diatom rich size fractions is again observed (Fig. 7), implying that radiolaria consistently form with a lower δ^{30}Si than diatoms at a similar location (Fig. 10, Table 2). At both sites, the 2–5 and 5–8 μm fractions have high δ^{30}Si, and Fig. 6 shows that they are the fractions with most pure diatom silica. By assuming the average δ^{30}Si of the 2–8 μm size range is exclusively diatom, an appropriate upper size limit can be determined: The δ^{30}Si of the 8–12 μm and 12–20 μm size fractions at both sites is within error (internal or external) of the 2–8 μm range, and so are considered to record diatom δ^{30}Si. At both sites the 20–41 μm fraction is outside this range, and so the 2–20 μm fraction in this region, as for the Antarctic Peninsula, is considered the most representative of diatom δ^{30}Si. Although the 41–50 μm fraction at TAN124 is within error of the 2–20 μm range, it will likely be subject to the previously discussed issues with sample heterogeneity and as such is best excluded.

For all NZ sites where a resolvable offset is observed, the 2–20 μm fraction has a higher δ^{30}Si than the 20–63 μm fraction, and is taken to record diatom δ^{30}Si (Fig. 9, Electronic Annex 2). The magnitude of the offset between the two fractions at these sites is qualitatively related to the type and amount of non-diatom component present, but is again much greater than would be predicted from the area analysis (Figs. 6e and 9, Electronic Annex 2). The two sites with the greatest δ^{30}Si offset, NZ4 (offset $= -1.22‰$) and NZ5 (offset $= -0.63‰$) are the only two sites containing sponge spicules in the 20–63 μm fraction (both 1% by area), with NZ4 having a larger radiolarian component (16%) than NZ5 (1%). This is consistent with the larger offset at NZ4, but the low levels of contamination would not be ex-

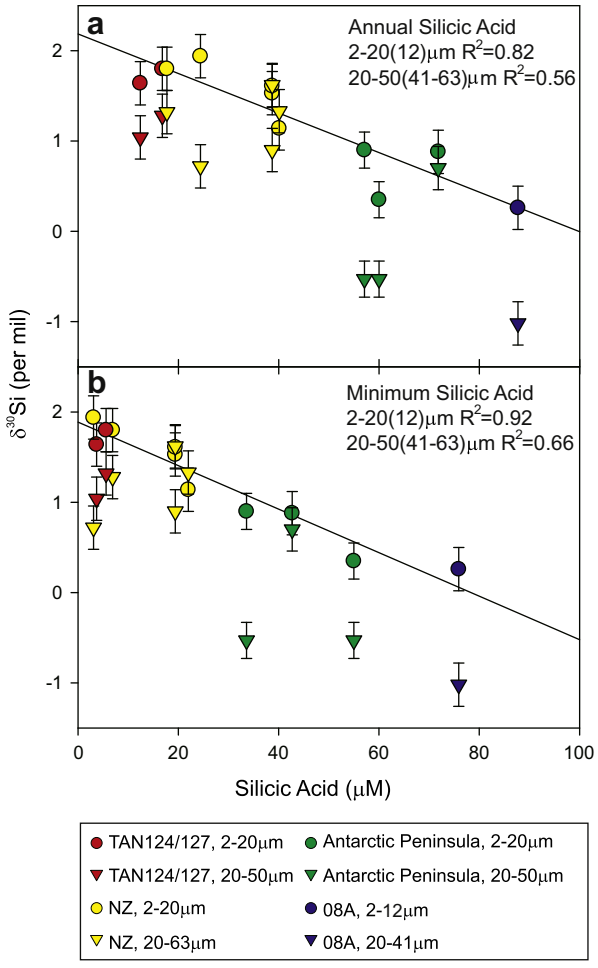

Fig. 9. Core top δ^{30}Si of size ranges comprised of predominantly diatoms (circles) or a combination of diatoms and non-diatom components (triangles); (a) Compared to the annual surface water silicic acid concentration at each site taken from the nearest grid point of the World Ocean Atlas, 2005 (with the exception of Site 391 which is from Clarke et al. (2008)); (b) Compared to the minimum silicic acid concentration observed yearly, taken from monthly surface water silicic acid concentrations at the nearest grid point in the World Ocean Atlas, 2005 (again with the exception of site 391 from Clarke et al. (2008)). There is a poorer correlation using the larger size fractions, in keeping with our assertion that these are affected by non-diatom silicon. There is a better correlation between the diatom δ^{30}Si size range and minimum silicic acid concentration than with annual silicic acid concentration.

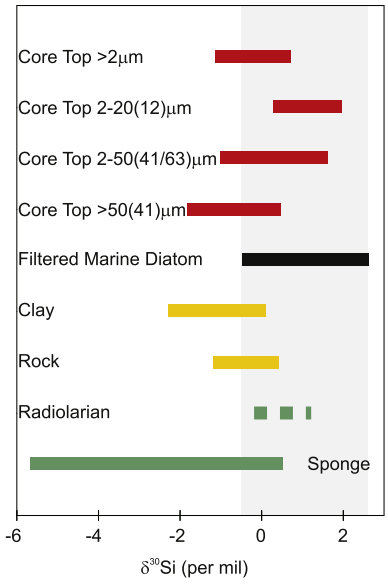

Fig. 10. Published δ^{30}Si ranges for the type of non-diatom components present in our core tops and for diatoms filtered from the modern ocean. Also plotted are the δ^{30}Si ranges of size fractions from the core tops which contain diatoms (2–20 or 2–12 μm), clay + diatoms (<2 μm, but TAN 127 not included), radiolaria/sponges/clastics + diatoms (20–41/50/63 μm) and radiolaria/clastics (>41/50 μm). See Section 4.2 for details of size fraction contents at each site. Filtered marine diatom δ^{30}Si between −0.5 and +2.6‰ (grey shading, Varela et al., 2004; Cardinal et al., 2007; Fripiat et al., 2011a; data from top 100 m of the water column only). It should be noted that inclusion of radiolarian tests in this filtered opal cannot be ruled out (Cardinal et al., 2007). Sponge δ^{30}Si between +0.5 and −5.7‰ (Hendry and Robinson, 2012). Clay δ^{30}Si from +0.1‰ to −2.3‰ (Basile-Doelsch, 2006). Sedimentary, mafic and felsic rock δ^{30}Si observations between ~+0.4 and −1.2‰, −0.1 and −0.4‰, and +0.4‰ and −0.4‰, respectively (Reynolds, 2011). Few measurements of radiolarian δ^{30}Si exist: Ding et al. (1996), measure three samples of radiolaria from mid-Pacific sediments (δ^{30}Si of +0.3 to −0.2‰), and a set of radiolarian siliceous rocks from the Cambrian to Jurassic (δ^{30}Si of +0.8‰ to −0.6), and Wu et al. (1997) measure a range of +0.2 to +1.2‰ in downcore Pacific samples. The scarcity of measurements and dominance of geological samples makes it difficult to assess the actual range of radiolarian δ^{30}Si.

Table 2
Diatom/radiolarian δ^{30}Si offsets.

Site	2–20 μm averaged (diatom)	>50 μm/>41 μm (radiolarian)	Offset
383	0.9	−1.21	2.11
391	0.72	−1.84	2.56
127	1.64	0.45	1.19
124	1.80	−0.05	1.85

pected to produce an offset at all if the sample analysed had silica ratios equivalent to the area analysis. Of NZ 6, 7 and 11, NZ7 has the largest radiolarian contribution to 20–63 μm silica (9%) and is the only one of the three to show any offset.

The pattern of δ^{30}Si across size fractions from downcore analysis of 1090 is very similar to TAN124 and 127, which are located in a similar oceanographic setting north of the modern Polar Front (Figs. 1 and 8), indicating that this relationship holds as far back as 36 Ma. The δ^{30}Si of the 1090 20–41 μm fractions is generally lower than that of the modern core tops, suggesting more influence from non-diatom silica. For these downcore samples the 2–20 μm range is again the most appropriate for targeting diatom δ^{30}Si.

For core top sediments analysed in this study, the 2–20 μm appears as the size fraction most consistently repre-

Table 3
Mass balance calculations of the percentage radiolarian silica required to produce published palaeoceanographic offsets.

Paper	Time period	Maximum δ^{30}Si (diatom) (‰)	Minimum δ^{30}Si (‰)	Offset (‰)	Required radiolarian contamination (%)
De La Rocha et al. (1998)	LGM	1.5	0.8	0.7	35
Brzezinski et al. (2002)	0–300 Ka	2	1	1	50
Beucher et al. (2007)	LGM	1.7	1.1	0.6	30

sentative of diatom δ^{30}Si. However, the low δ^{30}Si of the 12–20 μm fraction at 08A highlights the need to tailor size fraction selection to sediment composition. Another important observation is the extent to which very minor amounts of sponge and radiolarian silica can offset the δ^{30}Si of a sample which under the microscope appears to be almost entirely composed of diatom silica. The presence of non-diatom material down to relatively small size is not a result of fragmentation of these components during microseparation (Electronic Annex 1), and has previously been noted by Singer and Shemesh (1995) and Crosta and Shemesh (2002), who remove the >20 μm fraction from their samples to avoid radiolarian contamination. Samples should be carefully examined and the appropriate size fractions selected prior to analysis to ensure that measured δ^{30}Si represents robustly diatom δ^{30}Si. An initial test of δ^{30}Si from a set of size fractions in representative downcore samples may be useful in such an assessment. Additionally, running two size fractions (e.g. the 2–10 μm and 10–20 μm) from the same sample at selected intervals will help to ensure measured δ^{30}Si consistently reflects diatom δ^{30}Si downcore.

Diatom species composition has been suggested as a factor which may influence δ^{30}Si (De La Rocha, 2006). The species composition of our size fractions is shown in Electronic Annex 3. Size fractions in the 2–20 μm range, with consistent δ^{30}Si, contain different diatom assemblages, indicating that diatom vital effects are unlikely to affect δ^{30}Si. However, because it was not possible to separate 100% species specific size fractions we cannot as yet draw any firm conclusions regarding this issue.

4.1.1. Implications for published δ^{30}Si records

The previously highlighted potential for common sedimentary components to bias measured δ^{30}Si away from diatom δ^{30}Si could lead to misrepresentation of palaeoenvironmental changes. This is especially significant as geological studies tend to focus on climatic boundaries, when the abundance of taxa such as radiolaria and sponges relative to diatoms may change rapidly, as well as the ratio of

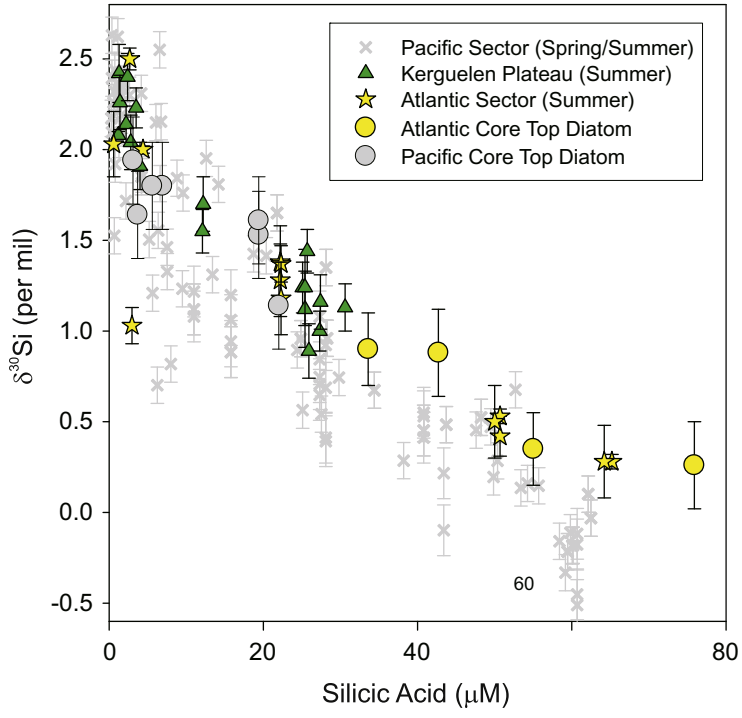

Fig. 11. Core top diatom δ^{30}Si (2–20 μm or 2–12 μm) compared to filtered diatom δ^{30}Si collected during *in situ* studies from the top 100 m of the water column (Varela et al., 2004; Cardinal et al., 2007; Fripiat et al., 2011a). Core top diatom δ^{30}Si is plotted against minimum annual silicic acid concentration, and the filtered diatom δ^{30}Si against the silicic acid concentration measured at the time of sampling. Core top diatom δ^{30}Si and filtered diatom δ^{30}Si are remarkably consistent, especially when they are from the same ocean basin.

biogenic to non biogenic components such as clay. Additionally, downcore, the preservation of biogenic opal may change significantly, and of particular relevance to the separation of diatoms from radiolarian/sponges, the degree of fragmentation may change, something which can complicate the separation of radiolarian and diatom silica.

Low δ^{30}Si is generally recorded at the Last Glacial Maximum (LGM) (De La Rocha et al., 1998; Brzezinski et al., 2002). The LGM is also frequently defined by a peak in relative abundance of the radiolarian *Cycladophora davisiana* (De La Rocha et al., 1998), raising the possibility of an increased glacial contribution from low δ^{30}Si radiolarian silica. Examples of negative offsets observed during glacial stages in published records are 1.5‰ (De La Rocha et al., 1998), 1.7‰ (Beucher et al., 2007) and 2‰ (Brzezinski et al., 2002) (Table 3), and would require 30–50% radiolarian contribution to explain the entirety of the offset (calculated by taking diatom δ^{30}Si to be the most positive value observed in the records and offsetting this by −2‰ (Table 2) to give the radiolarian δ^{30}Si). It seems unlikely that such levels of contamination are present in any of the published records, since authors are generally careful to eliminate non-diatom components. Although it is not always clear exactly what size fraction has been analysed, diatom δ^{30}Si studies generally follow methods such as those of Shemesh et al. (1988), Singer and Shemesh (1995), and Crosta and Shemesh (2002), which use the <20 μm (Singer and Shemesh, 1995; Crosta and Shemesh, 2002), or <38 μm (Shemesh et al., 1988) fractions, and should exclude the majority of radiolarian or sponge silica.

4.2. Diatom δ^{30}Si as a proxy for silicic acid utilisation

In Section 4.1 the size range most representative of diatom δ^{30}Si was determined to be the 2–20 μm (or 2–12 μm for 08A) and in this section either the δ^{30}Si of this size fraction or the mass balanced δ^{30}Si from size fractions within this range will be referred to as core top diatom δ^{30}Si.

Core top diatom δ^{30}Si correlates well with both the annual average silicic acid concentration and the minimum annual silicic acid concentration at each site (Fig. 9, $R^2 = 0.82$ and 0.92 respectively). The silicic acid concentrations were estimated from the nearest grid point to the core site in the World Ocean Atlas, 2005. The poorer correlation between silicic acid concentration and the 20–50/20–41/20–63 μm (depending which was measured at each site) δ^{30}Si (Fig. 9, $R^2 = 0.55$ or 0.66) confirms that this fraction should be excluded from silica analysed in studies targeting silicic acid utilisation. Fig. 9b shows a particularly robust relationship between core top diatom δ^{30}Si and the minimum surface water silicic acid concentration when the correct size fraction of sedimentary silica is analysed, validating the use of diatom δ^{30}Si as a proxy for silicic acid utilisation and highlighting the need for careful size fraction selection. Core top δ^{30}Si is remarkably consistent with mixed layer filtered diatom δ^{30}Si from the equivalent sector of the Southern Ocean (Fig. 11), indicating that surface diatom δ^{30}Si is faithfully recorded in the sediments, with minimal effect of either dissolution, which should act to increase the δ^{30}Si of the diatom opal (Demarest et al., 2009), or of early diagenesis. Minimal effect of dissolution is consistent with sediment trap δ^{30}Si and filtered diatom δ^{30}Si-depth profiles, which have found no evidence for δ^{30}Si modification during sinking (Varela et al., 2004; Cardinal et al., 2007; Fripiat et al., 2011a). This is again supportive of the qualitative use of diatom δ^{30}Si as a proxy for silicic acid utilisation. It should be noted that as we plot our core top data against minimum silicic acid concentration, they are less comparable to the spring data measured in the Pacific by Cardinal et al. (2005), and the spring data included in Varela et al. (2004). This likely explains why a portion of these filtered data are offset somewhat from the core top δ^{30}Si data.

However, there are still some important considerations which should be taken into account when interpreting diatom δ^{30}Si records. Firstly, there is a significantly better correlation ($p > 0.95$) between core top diatom δ^{30}Si and minimum silicic acid concentration (Fig. 9b) compared to the mean annual silicic acid concentration (Fig. 9a) ($R^2 = 0.92$, 0.82 respectively). The significance of the difference in goodness-of-fit between the minimum and mean annual models was estimated using a bootstrapping method which accounts for the error bars on the δ^{30}Si measurements (Electronic Annex 4). Unfortunately, we have been unable to obtain good error estimates for the silicic acid concentrations from the World Ocean Atlas (2005), which has precluded us taking these into account when testing this significance. This difficulty stems from two main issues. Firstly, the World Ocean Atlas is a gridded field, meaning that for a number of our core top locations, the silicic acid estimates are based on one or fewer actual measurements. Secondly, the error bars which are quoted in the World Ocean Atlas are determined not only by the actual variation in silicic acid on an annual basis, but by both the number of measurements and, for the mean annual estimates, the seasonality of a given location, making their inclusion rather uninformative. Nevertheless, the better correlation between minimum silicic acid concentration and 2–20 μm diatom δ^{30}Si suggests that sedimentary diatom δ^{30}Si documents seasonal diatom silicic acid utilisation. This could be explained by sedimentary diatom δ^{30}Si recording silicic acid utilisation only at the time when diatoms are growing (e.g. during summer stratification in the Southern Ocean, when silicic acid is driven to a minimum and δ^{30}Si to high values (Varela et al., 2004; Fripiat et al., 2011c)), whereas average annual silicic acid concentration may include large portions of the year when diatom production is minimal and surface silicic acid concentration is high (e.g. during winter mixing), and so will be biased towards higher silicic acid concentrations. The extent to which the annual silicic acid concentration is offset from the minimum will be dependent on the degree of seasonality at a given location, creating the observed variation in the R^2: At sites such as 383 and 385, the minimum silicic acid concentration is much lower than the annual average indicating there is a seasonal nature to diatom driven silicic acid drawdown (Table 1). In contrast at core top locations where production is either more continuous throughout the year (e.g. near TAN127/124 (Sigmon et al., 2002)) or where the extent of seasonal drawdown is very small (e.g. 391 (Clarke et al., 2008)), the annual silicic acid concentration is more similar

to the minimum (Table 1). That the seasonal maximum of silicic acid utilisation is being recorded in sedimentary diatom δ^{30}Si is an important point to acknowledge when interpreting downcore records, since the season of diatom productivity may be as little as only 3 months in some regions south of the Polar Front (Sigmon et al., 2002). If diatom δ^{30}Si records are produced from cores located in regions where silicic acid uptake is highly seasonal or if seasonality changes through time, changes in silicic acid utilisation recorded by diatom δ^{30}Si may exaggerate the change in silicic acid concentration of the wider, annually integrated surface ocean. This is also something which

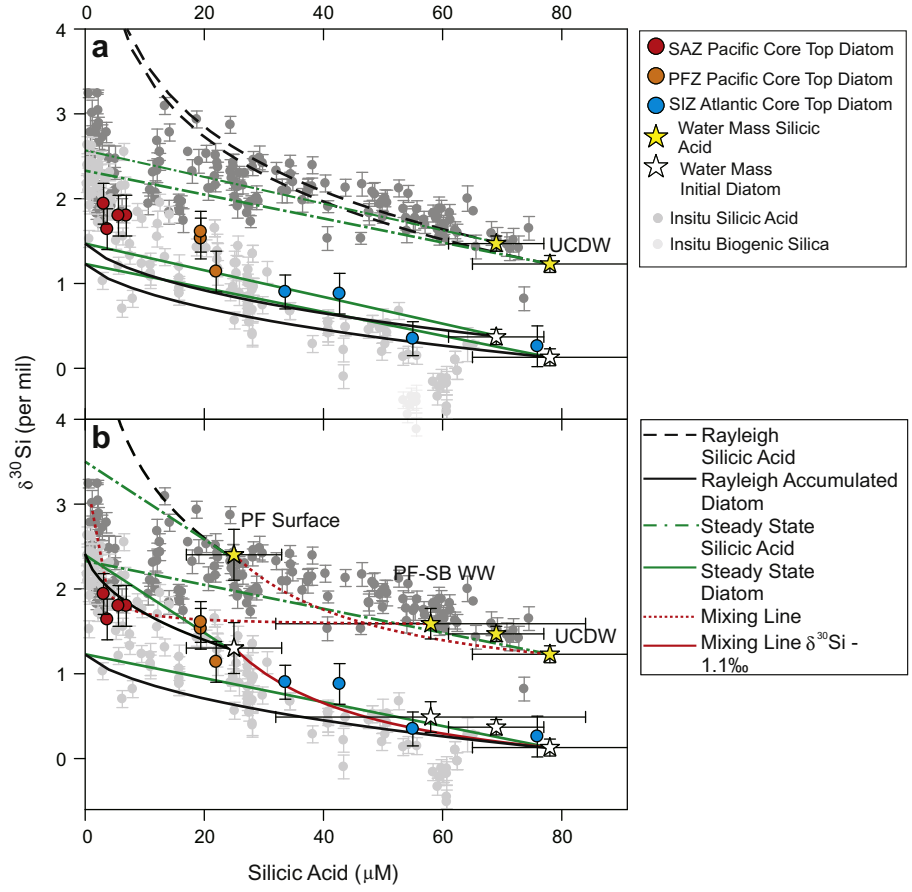

Fig. 12. Core top diatom δ^{30}Si (coloured circles), shown with filtered diatom δ^{30}Si and silicic acid δ^{30}Si measured during *in situ* studies of the Southern Ocean (top 100 m of the water column, grey circles; Varela et al., 2004; Cardinal et al., 2005, 2007; De La Rocha et al., 2011; Fripiat et al., 2011a,b,c); (a) With Rayleigh and steady state δ^{30}Si evolution of silicic acid and diatom silica (accumulated product for the Rayleigh model), assuming a fractionation factor of $-1.1‰$ and taking the silicic acid concentration and δ^{30}Si of Upper Circumpolar Deep Water (UCDW) as initial conditions. Two estimates for UCDW composition were considered; these encompass the range of values quoted for this water mass in the literature: UCDW (Pacific) = 78 ± 13 μM, 1.23 ± 0.13‰ (in Fripiat et al., 2011b, from the data of Cardinal et al., 2005) and UCDW (Atlantic) = 69 ± 8 μM, 1.47 ± 0.37‰ (Fripiat et al., 2011b) (error bars as quoted in Fripiat et al., 2011b). Neither model can explain the range of δ^{30}Si observed in our core top data, particularly at sites north of the Polar Front with silicic acid concentrations of <20 μM; (b) Rayleigh and Steady state evolutions, but in this case with initial conditions taken as either the Pacific UCDW composition, or an estimate of the Pacific Polar Front surface water composition (25 ± 8 μM, 2.4 ± 0.3‰; PF-Surface; calculated using data from 60–63°S in Varela et al., 2004, error bars are 1σSD, n = 16). The mixing line between these two end members (red dashed line between UCDW and PF-surface stars) can be taken to represent the source waters from which diatom silicification occurs in the Southern Ocean. Rayleigh or steady state fractionation curves from anywhere on this mixing line will plot between those shown for UCDW and PF surface. These fractionation lines satisfactorily explain the variation in δ^{30}Si of our core tops, and the majority of the filtered diatom δ^{30}Si. Also plotted is a mixing line between the Pacific Winter Water (averaged between the Polar Front and the Southern Boundary of the Antarctic Circumpolar Current; PF–SB WW; Cardinal et al., 2005; Fripiat et al., 2011b, error bars as quoted in Fripiat et al., 2011b), and an evolved composition from north of the Polar Front (1 μM, 3‰, based on the estimate of Fripiat et al. (2011b); no data are available for summer conditions north of the Polar Front in the Pacific). This fractionation and mixing can account for the low apparent fractionation factor at low silicic acid concentrations. It should be noted that these mixing lines would not look significantly different using Atlantic end member estimates, but since the majority of our core tops are located in the Pacific, we have chosen to use the Pacific end members. SAZ = Sub Antarctic Zone; PFZ = Polar Front Zone; SIZ = Seasonal Ice Zone; PF = Polar Front; PF–SB = Polar Front–Southern Boundary (of the Antarctic Circumpolar Current); WW = Winter Water. (For interpretation of the references to colour in this figure legend, the reader is referred to the web version of this article.)

Table 4
Estimated ε and $\delta^{30}Si(OH)_{4\,initial}$.

Data set	Fractionation factorε (‰)	Initial silicic acid $\delta^{30}Si(OH)_{4\,initial}$ (‰)	R^2
2–20 (12) μm core top	-1.9 ± 0.2 (steady state)	2.0 ± 0.1(steady state)	0.92
UCDW Fripiat et al., 2011b	-1.8 ± 0.2 (Rayleigh)	2.2 ± 0.1 (Rayleigh)	0.88
2–20(12)μm core top	-2.2 ± 0.2 (steady state)	1.9 ± 0.1(steady state)	0.92
UCDW Cardinal et al., 2005	-2.1 ± 0.2 (Rayleigh)	2.2 ± 0.1 (Rayleigh)	0.92
Top 100 m silicic acid compilation (Frip UCDW)	-0.9 ± 0.1 (steady state)	1.6 ± 0.05 (steady state)	0.48
Top 100 m silicic acid compilation (Card UCDW)	-1.1 ± 0.1 (steady state)	1.4 ± 0.05 (steady state)	0.47
Mixed layer filtered diatoms (Frip UCDW)	-2.5 ± 0.1 (steady state)	2.0 ± 0.05 (steady state)	0.82
Mixed layer filtered diatoms (Card UCDW)	-3.2 ± 0.1 (steady state)	2.0 ± 0.05 (steady state)	0.82

should be kept in mind when interpolating results between cores which are located in different oceanic regimes.

Secondly, the reliability of quantitative silicic acid reconstructions from diatom $\delta^{30}Si$ pivots on the assumption that simple Rayleigh or steady state models, with a single silicic acid concentration/$\delta^{30}Si$ source term and a consistent diatom fractionation factor are sufficient to describe the Southern Ocean $\delta^{30}Si$ distribution. This would appear not to be the case for our core top data.

Rayleigh Fractionation is characterised by the following equations;

$$\delta^{30}Si(OH)_4 = \delta^{30}Si(OH)_{4\,initial} + {}^{30}\varepsilon \ln f \quad (1)$$

$$\delta^{30}Si\text{–}bSiO_2 = \delta^{30}Si(OH)_4 + {}^{30}\varepsilon \quad (2)$$

$$\delta^{30}Si\text{–}bSiO_{2\,acc} = \delta^{30}Si(OH)_{4\,initial} - {}^{30}\varepsilon(f\ \ln f/1-f) \quad (3)$$

where $Si(OH)_4$ is silicic acid, $Si(OH)_{4\,initial}$ is initial silicic acid, $bSiO_2$ is diatom silica, $bSiO_{2\,acc}$ is accumulated diatom silica, and f is the fraction of silicic acid remaining in the surface ocean. In this model, sedimentary diatom silica should reflect the accumulated diatom $\delta^{30}Si$ (Eq. (3)).

For the steady state model,

$$\delta^{30}Si(OH)_4 = \delta^{30}Si(OH)_{4\,initial} - {}^{30}\varepsilon(1-f) \quad (4)$$

$$\delta^{30}Si\text{–}bSiO_2 = \delta^{30}Si(OH)_{4\,initial} + {}^{30}\varepsilon f \quad (5)$$

In order to test how well core top diatom $\delta^{30}Si$ fits these models, an estimate of the initial conditions from which fractionation occurs must be made. Upper Circumpolar Deepwater (UCDW) is probably the most ubiquitous ultimate source of silicic acid to the mixed layer, either by upwelling or Ekman Transport, over the latitudinal range of our Southern Ocean core tops (Whitworth III et al., 1994; Pollard et al., 2002; Clarke et al., 2008; Fripiat et al., 2011b) (with the exception of 08A where Lower Circumpolar Deepwater and Antarctic shelf water are more likely to control silicic acid supply (Whitworth III et al., 1994)). We have therefore used two different estimates of the silicic acid concentration/$\delta^{30}Si$ signature of UCDW (Cardinal et al., 2005; Fripiat et al., 2011b) to represent initial conditions (Fig. 12a). The expected Rayleigh and steady state $\delta^{30}Si$ evolution from UCDW were calculated assuming a fractionation factor of -1.1‰ (De La Rocha et al., 1997), and are shown compared to our core top diatom $\delta^{30}Si$ in Fig. 12a. Values of ${}^{30}\varepsilon$ and initial silicic acid $\delta^{30}Si$ were also calculated (Table 4) from the gradient and intercept of the linear regression of core top diatom $\delta^{30}Si$ against either f or $(f \ln f)/(1-f)$ for steady state and Rayleigh accumulated opal, respectively (Eqs. (3) and (5)). f was set as the minimum silicic acid concentration at each site divided by the UCDW concentration. Quoted errors for ${}^{30}\varepsilon$ and $\delta^{30}Si(OH)_{4\,initial}$ are ±1SE on the gradient and intercept of the regression line respectively.

Values of ${}^{30}\varepsilon$ estimates from our core top diatom $\delta^{30}Si$ vs. minimum silicic acid concentration are between -1.9 ± 0.2‰ and -2.2 ± 0.2‰ (both models are in agreement, Table 4). The gradient of the core top $\delta^{30}Si$ is therefore too large to be compatible with a fractionation factor of -1.1‰ using these simple models, explaining the lack of coherence with any of the model fractionations illustrated in Fig. 12a. This is highlighted by the high estimates of $\delta^{30}Si(OH)_{4\,initial}$ from the core top diatom $\delta^{30}Si$ (Table 4). *In situ* studies have also observed a steeper than expected increase in surface filtered diatom $\delta^{30}Si$ with silicic acid concentration when using ${}^{30}\varepsilon = -1.1$‰ and simple single source models (Varela et al., 2004; Cardinal et al., 2007; Fripiat et al., 2011a). Varela et al. (2004) estimate ${}^{30}\varepsilon$ to be -2.1 ± 0.2‰ for filtered biogenic silica, using a steady state model starting from 65 μM, which is remarkably consistent with our estimate from the core top data. Taking all the Southern Ocean mixed layer filtered diatom $\delta^{30}Si$ data published to date, and using either UCDW estimate as a starting point, the steady state model yields ${}^{30}\varepsilon = -2.5 \pm 0.1$‰ or -3.2 ± 0.1‰ (Table 4), which is again very high. On the contrary ${}^{30}\varepsilon$ estimates made in the same way assuming the single source steady state model and published silicic acid $\delta^{30}Si$ from the Southern Ocean mixed layer are -0.9 ± 0.1‰ or -1.1 ± 0.1‰. This is very similar to the compiled Antarctic Circumpolar Current ${}^{30}\varepsilon$ estimate of -1.2 ± 0.2‰ from Fripiat et al. (2011c), despite the fact that this estimate includes studies which considered fractionation from a variable source targeted at the specific location being considered (Cardinal et al., 2005; Fripiat et al., 2011c). The large difference in ${}^{30}\varepsilon$ estimates from core top diatom $\delta^{30}Si$ and silicic acid $\delta^{30}Si$ leads to an increase in the apparent fractionation factor (offset between $\delta^{30}Si$ of silicic acid and of core top/filtered diatoms) with increasing latitude (silicic acid concentration) (Varela et al., 2004; Cardinal et al., 2007; Fripiat et al., 2011a) which can be clearly seen in Fig. 12. Such observations demonstrate that the simple fractionation models cannot account for the $\delta^{30}Si$ distribution recorded in Southern Ocean sediments.

Two main hypotheses on the cause of such deviations from the idealised models can be considered. Firstly, the

assumption of a single source is likely to be wrong, given the significant mixing which occurs both vertically and horizontally in the Southern Ocean mixed layer from which diatoms produce their silica (Cardinal et al., 2005, 2007; Fripiat et al., 2011b). Secondly, the assumption of a constant fractionation factor with latitude may be incorrect (Varela et al., 2004; Cardinal et al., 2007; Hendry and Robinson, 2012). Although a change in the diatom fractionation factor with latitude cannot be ruled out, it can be demonstrated that when the effects of water mass mixing are taken into account, variation in the core top diatom δ^{30}Si can be satisfactorily explained using a constant fractionation factor of approximately $-1.1‰$ (Fig. 12b).

Fripiat et al. (2011a) have shown that in the Atlantic Sector of the Southern Ocean, the sub-surface (Winter Water) silicic acid concentration and δ^{30}Si plot on a mixing line between the characteristic signatures of UCDW and the seasonally depleted mixed layer. This Winter Water may be considered the starting point for diatom silicon isotope fractionation over large areas of the Southern Ocean (Cardinal et al., 2005; De La Rocha et al., 2011; Fripiat et al., 2011a). Simplistically, a mixing line of this type, for example between Pacific UCDW and the Polar Front surface ocean (Fig. 12b), can be taken to represent the possible range of silicic acid concentration and δ^{30}Si which may be present at the beginning of seasonal diatom production (this line would not appear significantly different using Atlantic end member estimates from Fripiat et al. (2011a)). Steady state or Rayleigh fractionation models can then be used to calculated the evolution of silicic acid and diatom δ^{30}Si from anywhere on this spectrum of initial conditions (following Cardinal et al. (2005) and Fripiat et al. (2011a)). Any such fractionation will plot somewhere between the fractionation lines from UCDW and the Polar Front surface water silicic acid which are illustrated in Fig. 12b. Our core top diatom δ^{30}Si data are compatible with such a model (i.e. fractionation, either Rayleigh or steady state, from an initial water mass composition described by mixing between UCDW and surface waters at the Polar Front) of Southern Ocean δ^{30}Si fractionation (Fig. 12b), which also describes much of the variation in surface water silicic acid and filtered diatom δ^{30}Si from *in situ* studies (with the exception of some very low filtered diatom δ^{30}Si values at high silicic acid concentration in the Pacific). In particular, this description of the system can provide an explanation of the relatively high core top diatom δ^{30}Si at silicic acid concentrations <20 μM (Fig. 12b). The fit between this mixing model and our core top diatom δ^{30}Si is in good agreement with Fripiat et al. (2011a). Their modelling of seasonal mixed layer δ^{30}Si evolution at the Polar Front shows that biogenic silica exported from the mixed layer can be satisfactorily replicated by a Rayleigh accumulated product. As demonstrated by Fripiat et al. (2011a,b), the unexpectedly low δ^{30}Si of the surface water silicic acid at low silicic acid concentrations, which also contributes to the low apparent fractionation factor, can be explained by mixing of an evolved water mass having very low silicic acid concentration and high δ^{30}Si (driven by diatom production), with subsurface waters sourced from the Polar Front having higher silicic acid concentration and lower δ^{30}Si. This is illustrated on Fig. 12b by a mixing line between the Pacific Winter Water (averaged between the Polar Front and the Southern Boundary of the ACC; in Fripiat et al. (2011b), from the data of Cardinal et al. (2005)) and a hypothetical mixed layer from north of the Polar Front (1 μM, $3‰$, based on the estimate of Fripiat et al. (2011b); no data are available for summer conditions north of the Polar Front in the Pacific). Such a mixing line is a good example of how the relationship between physical mixing and biological uptake might control the δ^{30}Si distribution in the surface waters of the Southern Ocean.

Since dissolution acts to increase the δ^{30}Si of diatom silica (Demarest et al., 2009), it could provide an alternative explanation for the relatively high δ^{30}Si, and the small apparent fractionation factor, at core top locations with silicic acid <20 μM. However, good agreement between our core top diatom δ^{30}Si and mixed layer filtered diatom δ^{30}Si, and the preservation of surface diatom δ^{30}Si signatures in both deep sediment traps (Varela et al., 2004) and through depth profiles of filtered diatoms (Cardinal et al., 2007; Fripiat et al., 2011a) all argue against dissolution as the driver of these relatively high values. Additionally, the modelling results of Fripiat et al. (2011a) indicate that there should be no significant effect of dissolution on the δ^{30}Si of accumulated diatom silica.

Reconstruction of surface water silicic acid concentrations from diatom δ^{30}Si does appear to be robust (Fig. 9). However, any attempt to fully quantify changes in the degree of silicic acid utilisation will be subject to major uncertainties regarding the initial surface water mass composition and mixing regime. A particularly optimistic note from this study is that the diatom δ^{30}Si signal appears unaltered by dissolution over million year timescales (Fig. 8).

5. CONCLUSIONS

A consistent size-δ^{30}Si pattern, related to the proportions of diatom and non-diatom components in a sample, has been demonstrated. This study highlights the great potential for small amounts of non-diatom silica to significantly offset measured δ^{30}Si to lower values than diatom δ^{30}Si. In order to create reliable downcore records of diatom δ^{30}Si, it is essential to eliminate such contamination by selecting the correct size fraction for analysis. In general the 2–20 μm fraction has been found most appropriate for core tops in this study, although this is not a hard and fast rule, and rather must be tailored to the sediment composition of each sample set.

When a pure diatom size fraction is selected, an extremely good correlation with surface water minimum annual silicic acid concentration is documented ($R^2 = 0.92$). In comparison, larger size fractions (~20–50 μm) exhibit a poorer correlation ($R^2 = 0.66$), again emphasising the need for size targeted analyses.

Correlation with surface silicic acid concentration, and a good agreement between core top diatom δ^{30}Si and surface filtered diatom δ^{30}Si, are highly supportive of the use of sedimentary diatom δ^{30}Si as a proxy for surface water silicic acid utilisation and indicate no significant effect of dissolu-

tion or early diagenesis. The better correlation with minimum annual silicic acid reflects the fact that diatom δ^{30}Si records the seasonal extent of silicic acid utilisation by diatoms, which should be kept in mind when interpreting diatom δ^{30}Si records.

Core top diatom δ^{30}Si can be satisfactorily explained using steady state or Rayleigh fractionation without the need to invoke a variable diatom fractionation factor, as long as changes in the silicic acid concentration and δ^{30}Si from which diatom uptake occurs are properly accounted for i.e. it is not possible to model the entire Southern Ocean with a single set of initial conditions. This represents a major source of error in quantitative silicic acid utilisation reconstructions. However, it should not detract from the strong relationship which exists between sedimentary diatom δ^{30}Si and surface water silicic acid concentration, proving this to be a reliable qualitative proxy for silicic acid utilisation.

ACKNOWLEDGEMENTS

Many thanks to Nick Belshaw and Bastian Georg for their help with silicon isotope analysis, to Jenny Pike for her training in diatom identification, to Jorn Bruggeman for his statistical analyses, and to George Swann and Fatima Mokadem for their help with lab protocols/setup. Thank you to Greg de Souza and two anonymous reviewers for their insightful comments, which have significantly improved this manuscript. Thanks to the Ocean Drilling Program for supplying downcore samples from site 177-1090. The Oxford isotope geochemistry lab is supported by an ERC grant to Halliday. This work was carried out as part of Natural Environmental Research Council (NERC) Grant NE/F005296/1, and Antarctic Peninsula core tops collected thanks to the Antarctic Funding Initiative Grant AFI4-02.

APPENDIX A. SUPPLEMENTARY DATA

Supplementary data associated with this article can be found, in the online version, at http://dx.doi.org/10.1016/j.gca.2012.08.002.

REFERENCES

Baines S. B., Twining B. S., Brzezinski M. A., Nelson D. M. and Fisher N. S. (2010) Causes and biogeochemical implications of regional differences in silicification of marine diatoms. *Global Biogeochem. Cycles* **24**.

Basile-Doelsch I. (2006) Si stable isotopes in the Earth's surface. A review. *J. Geochem. Explor.* **88**, 252–256.

Beucher C. P., Brzezinski M. A. and Crosta X. (2007) Silicic acid dynamics in the glacial sub-Antarctic: Implications for the silicic acid leakage hypothesis. *Global Biogeochem. Cycles* **21**.

Beucher C. P., Brzezinski M. A. and Jones J. L. (2008) Sources and biological fractionation of silicon isotopes in the Eastern Equatorial Pacific. *Geochim. Cosmochim. Acta* **72**, 3063–3073.

Beucher C. P., Brzezinski M. A. and Jones J. L. (2011) Mechanisms controlling silicon isotope distribution in the Eastern Equatorial Pacific. *Geochim. Cosmochim. Acta* **75**, 4286–4294.

Brzezinski M. A., Pride C. J., Franck V. M., Sigman D. M., Sarmiento J. L., Matsumoto K., Gruber N., Rau G. H. and Coale K. H. (2002) A switch from $Si(OH)_4$ to NO-3 depletion in the glacial Southern Ocean. *Geophys. Res. Lett.* **29**, 5-1–5-4.

Buesseler K. O. (1998) The decoupling of production and particulate export in the surface ocean. *Global Biogeochem. Cycles* **12**, 297–310.

Cande S. C. and Kent D. V. (1995) Revised calibration of the geomagnetic polarity timescale for the Late Cretaceous and Cenozoic. *J. Geophys. Res.* **100**, 6094–6095.

Cardinal D., Alleman L. Y., Dehairs F., Savoye N., Trull T. W. and André L. (2005) Relevance of silicon isotopes to Si-nutrient utilization and Si-source assessment in Antarctic waters. *Global Biogeochem. Cycles* **19**, 1–13.

Cardinal D., Savoye N., Trull T. W., Dehairs F., Kopczynska E. E., Fripiat F., Tison J. and André L. (2007) Silicon isotopes in spring Southern Ocean diatoms: Large zonal changes despite homogeneity among size fractions. *Mar. Chem.* **106**, 46–62.

Channell J. E. T., Galeotti S., Martin E. E., Billups K., Scher H. D. and Stoner J. S. (2003) Eocene to Miocene magnetostratigraphy, biostratigraphy, and chemostratigraphy at odp site 1090 (sub-Antarctic South Atlantic). *Geol. Soc. Am. Bull.* **115**, 607–623.

Chapligin B., Leng M. J., Webb E., Alexandre A., Dodd J. P., Ijiri A., Lucke A., Shemesh A., Abelmann A., Herzschuh U., Longstaffe F. J., Heyer H., Moschen R., Okazaki Y., Rees N. H., Sharpe Z. D., Sloane H. J., Sonzogni C., Swann G. E. A., Sylvestre F., Tyler J. J. and Yam R. (2011) Inter-laboratory comparison of oxygen isotope compositions from biogenic silica. *Geochim. Cosmochim. Acta* **75**, 7242–7256.

Clarke A., Meredith M. P., Wallace M. I., Brandon M. A. and Thomas D. N. (2008) Seasonal and interannual variability in temperature, chlorophyll and macronutrients in northern Marguerite Bay, Antarctica. *Deep Sea Res. Part II Top. Stud. Oceanogr.* **55**, 1988–2006.

Crosta X. and Shemesh A. (2002) Reconciling down core anticorrelation of diatom carbon and nitrogen isotopic ratios from the Southern Ocean. *Paleoceanography* **17**.

De La Rocha C. L. (2003) Silicon isotope fractionation by marine sponges and the reconstruction of the silicon isotope composition of ancient deep water. *Geology* **31**, 423–426.

De La Rocha C. L. (2006) Opal-based isotopic proxies of paleoenvironmental conditions. *Global Biogeochem. Cycles* **20**.

De La Rocha C. L., Brzezinski M. A. and Deniro M. J. (1997) Fractionation of silicon isotopes by marine diatoms during biogenic silica formation. *Geochim. Cosmochim. Acta* **61**, 5051–5056.

De La Rocha C. L., Brzezinski M. A., Deniro M. J. and Shemesh A. (1998) Silicon-isotope composition of diatoms as an indicator of past oceanic change. *Nature* **395**, 680–683.

De La Rocha C. L., Brzezinski M. A. and Deniro M. J. (2000) A first look at the distribution of the stable isotopes of silicon in natural waters. *Geochim. Cosmochim. Acta* **64**, 2467–2477.

De La Rocha C. L., Bescont P., Croguennoc A. and Ponzevera E. (2011) The silicon isotopic composition of surface waters in the Atlantic and Indian Sectors of the Southern Ocean. *Geochim. Cosmochim. Acta* **75**, 5283–5295.

Demarest M. S., Brzezinski M. A. and Beucher C. P. (2009) Fractionation of silicon isotopes during biogenic silica dissolution. *Geochim. Cosmochim. Acta* **73**, 5572–5583.

Ding T., Jiang S., Wan D., Li Y., Li J., Song H., Liu Z. and Yao X. (1996) *Silicon Isotope Geochemistry*. Geological Publishing House, Beijing, China.

Douthitt C. B. (1982) The geochemistry of the stable isotopes of silicon. *Geochim. Cosmochim. Acta* **46**, 1449–1458.

Elderfield H. and Rickaby R. E. (2000) Oceanic Cd/P ratio and nutrient utilization in the glacial Southern Ocean. *Nature* **405**, 305–310.

Ellwood M. J. and Hunter K. A. (1999) Determination of the Zn/Si ratio in diatom opal: A method for the separation, cleaning and dissolution of diatoms. *Mar. Chem.* **66**, 149–160.

Fripiat F., Cavagna A.-J., Dehairs F., De Brauwere A., André L. and Cardinal D. (2011a) Processes controlling the Si-isotopic composition in the Southern Ocean and application for paleoceanography. *Biogeosci. Discuss.* **8**, 10155–10185.

Fripiat F., Cavagna A.-J., Dehairs F., Speich S., André L. and Cardinal D. (2011b) Silicon pool dynamics and biogenic silica export in the Southern Ocean inferred from Si-isotopes. *Ocean Sci. Discuss.* **8**, 639–674.

Fripiat F., Cavagna A., Savoye N., Dehairs F., André L. and Cardinal D. (2011c) Isotopic constraints on the Si-biogeochemical cycle of the Antarctic Zone in the Kerguelen area (Keops). *Mar. Chem.* **123**, 11–22.

Georg R. B., Reynolds B. C., Frank M. and Halliday A. N. (2006) New sample preparation techniques for the determination of Si isotopic compositions using MC-ICPMS. *Chem. Geol.* **235**, 95–104.

Hendry K. R. and Rickaby R. E. M. (2008) Opal (Zn/Si) ratios as a nearshore geochemical proxy in coastal Antarctica. *Paleoceanography* **23**.

Hendry K. R. and Robinson L. F. (2012) The relationship between silicon isotope fractionation in sponges and silicic acid concentration: modern and core-top studies of biogenic opal. *Geochim. Cosmochim. Acta* **81**, 1–12.

Hendry K. R., Georg R. B., Rickaby R. E. M., Robinson L. F. and Halliday A. N. (2010) Deep ocean nutrients during the last glacial maximum deduced from sponge silicon isotopic compositions. *Earth Planet. Sci. Lett.* **292**, 290–300.

Kohfeld K. E., Quéré C. L., Harrison S. P. and Anderson R. F. (2005) Role of marine biology in glacial–interglacial CO_2 cycles. *Science* **308**, 74–78.

Leng M. J. and Barker P. A. (2006) A review of the oxygen isotope composition of lacustrine diatom silica for palaeoclimate reconstruction. *Earth Sci. Rev.* **75**, 5–27.

Leng M. J. and Sloane H. J. (2008) Combined oxygen and silicon isotope analysis of biogenic silica J. *Quaternary Sci.* **23**, 313–319.

Milligan A. J., Varela D. E., Brzezinski M. A. and Morel F. M. M. (2004) Dynamics of silicon metabolism and silicon isotopic discrimination in a marine diatom as a function of pCO_2. *Limnol. Oceanogr.* **49**, 322–329.

Minoletti F., Hermoso M. and Gressier V. (2009) Separation of sedimentary micron-sized particles for palaeoceanography and calcareous nannoplankton biogeochemistry. *Nat. Protoc.* **4**, 14–24.

Morley D. W., Leng M. J., Mackay A. W., Sloane H. J., Rioual P. and Battarbee R. W. (2004) Cleaning of lake sediment samples for diatom oxygen isotope analysis. *J. Paleolimnol.* **31**, 391–401.

Nelson D. M., Treguer P., Brzezinski M. A., Leynaert A. and Queguiner B. (1995) Production and dissolution of biogenic silica in the ocean: Revised global estimates, comparison with regional data and relationship to biogenic sedimentation. *Global Biogeochem. Cycles* **9**, 359–372.

Orsi A. H. (1995) On the meridional extent and fronts of the Antarctic Circumpolar Current Deep Sea Res. *Part I: Oceanographic Res. Papers* **42**, 641–673.

Pollard R. T., Lucas M. I. and Read J. F. (2002) Physical controls on biogeochemical zonation in the Southern Ocean. *Deep Sea Res. Part II Top. Stud. Oceanogr.* **49**, 3289–3305.

Ragueneau O., Savoye N., Del Amo Y., Cotten J., Tardiveau B. and Leynaert A. (2005) A new method for the measurement of biogenic silica in suspended matter of coastal waters: Using Si:Al ratios to correct for the mineral interference. *Cont. Shelf Res.* **25**, 697–710.

Reynolds B.C. (2011) Silicon Isotopes as tracers of terrestrial processes. Handbook of Environmental Isotope Geochemistry, In M. Baskaran (Ed.), (Vol. 1, pp. 87–104).

Reynolds B. C., Frank M. and Halliday A. N. (2008) Evidence for a major change in silicon cycling in the subarctic North Pacific at 2.73 Ma. *Paleoceanography* **23**.

Reynolds B. C., Aggarwal J., Andre L., Baxter D., Beucher C., Brzezinski M. A., Engstrom E., Georg R. B., Land M., Leng M. J., Opfergelt S., Rodushkin I., Sloane H. J., Van Den Boorn S. H. J. M., Vroon P. Z. and Cardinal D. (2007) An inter-laboratory comparison of Si isotope reference materials. *J. Anal. At. Spectrom.* **22**, 561.

Sarmiento J. L. and Toggweiler J. R. (1984) A new model for the role of the oceans in determining atmospheric pCO_2. *Nature* **308**, 621–624.

Shemesh A., Mortlock R. A., Smith R. J. and Froelich P. N. (1988) Determination of Ge/Si in marine siliceous microfossils: Separation, cleaning and dissolution of diatoms and radiolaria. *Mar. Chem.* **25**, 305–323.

Shemesh A., Burckle L. H. and Hays J. D. (1995) Late Pleistocene oxygen isotope records of biogenic silica from the Atlantic Sector of the Southern Ocean. *Paleoceanography* **10**, 179–196.

Sigman D. M. and Boyle E. A. (2000) Glacial/interglacial variations in atmospheric carbon dioxide. *Nature* **407**, 859–869.

Sigman D. M., Altabet M. A., Francois R., Mccorkle D. C. and Gaillard J. (1999) The Isotopic composition of diatom-bound nitrogen in Southern Ocean sediments. *Paleoceanography* **14**, 118.

Sigmon D. E., Nelson D. M. and Brzezinski M. A. (2002) The Si cycle in the pacific sector of the Southern Ocean: Seasonal diatom production in the surface layer and export to the deep sea. *Deep Sea Res. Part II Top. Stud. Oceanogr.* **49**, 1747–1763.

Singer A. J. and Shemesh A. (1995) Climatically linked carbon isotope variation during the past 430,000 years in Southern Ocean sediments. *Paleoceanography* **10**, 171.

Swann G. E. A. and Leng M. J. (2009) A review of diatom $\delta^{18}O$ in palaeoceanography. *Quatern. Sci. Rev.* **28**, 384–398.

Swann G. E. A., Leng M. J., Sloane H. J. and Maslin M. A. (2008) Isotope offsets in marine diatom $\delta^{18}O$ over the last 200 Ka. *J. Quat. Sci.* **23**, 389–400.

Takahashi T., Sutherland S. C., Sweeney C., Poisson A., Metzl N., Tilbrook B., Bates N., Wanninkhof R., Feely R. A., Sabine C., Olafsson J. and Nojiri Y. (2002) Global sea–air CO_2 flux based on climatological surface ocean pCO_2, and seasonal biological and temperature effects. *Deep Sea Res. Part II Top. Stud. Oceanogr.* **49**, 1601–1622.

Tréguer P., Nelson D. M., Van Bennekom A. J., Demaster D. J., Leynaert A. and Quéguiner B. (1995) The silica balance in the world ocean: A reestimate. *Science* **268**, 375–379.

Varela D. E., Pride C. J. and Brzezinski M. A. (2004) Biological fractionation of silicon isotopes in Southern Ocean surface waters. *Global Biogeochem. Cycles* **18**, Gb1047 1–Gb1047 8.

Whitworth, III, T., Nowlin, Jr., W. D., Orsi A. H., Locarnini R. A. and Smith S. G. (1994) Weddell Sea shelf water in the Bransfield Strait and Weddell-Scotia confluence. *Deep Sea Res. Part I Oceanogr. Res. Pap.* **41**, 629–641.

Wu S., Ding T., Meng X. and Bai L. (1997) Determination and geological implication of O–Si isotope of the sediment core in the CC area, the Pacific Ocean. *Chin. Sci. Bull.* **42**, 1462–1465.

Associate editor: Derek Vance